Published June 14, 2010

Homeostatic expansion of autoreactive immunoglobulin-secreting cells in the *Rag2* mouse model of Omenn syndrome

Barbara Cassani,[1] Pietro Luigi Poliani,[2] Veronica Marrella,[3,4] Francesca Schena,[5] Aisha V. Sauer,[6] Maria Ravanini,[2] Dario Strina,[3,4] Christian E. Busse,[7] Stephan Regenass,[8] Hedda Wardemann,[7] Alberto Martini,[5] Fabio Facchetti,[2] Mirjam van der Burg,[9] Antonius G. Rolink,[10] Paolo Vezzoni,[3,4] Fabio Grassi,[11,12] Elisabetta Traggiai,[5] and Anna Villa[3,6]

[1]Fondazione Humanitas per la Ricerca, 20089 Rozzano, Italy
[2]Department of Pathology, University of Brescia, 25100 Brescia, Italy
[3]Italian National Research Council (CNR)-Istituto Tecnologie Biomediche, 20090 Milan, Italy
[4]Istituto Clinico Humanitas, 20089 Rozzano, Italy
[5]Laboratory of Immunology and Rheumatic Disease, IGG, 16147 Genoa, Italy
[6]San Raffaele Telethon Institute for Gene Therapy (HSR-TIGET), 20132 Milan, Italy
[7]Max Planck Research Group Molecular Immunology, Max Planck Institute for Infection Biology, D-10117 Berlin, Germany
[8]Division of Clinical Immunology, University Hospital Zürich, Zürich CH 8091, Switzerland
[9]Department of Immunology, Erasmus MC, University Medical Center Rotterdam, 3015 GE Rotterdam, Netherlands
[10]Department of Biomedicine, University of Basel, 4031 Basel, Switzerland
[11]Institute for Research in Biomedicine, 6500 Bellinzona, Switzerland
[12]Dipartimento di Biologia e Genetica per le Scienze Mediche, Universita' degli Studi di Milano, 20133 Milan, Italy

Hypomorphic *RAG* mutations, leading to limited V(D)J rearrangements, cause Omenn syndrome (OS), a peculiar severe combined immunodeficiency associated with autoimmune-like manifestations. Whether B cells play a role in OS pathogenesis is so far unexplored. Here we report the detection of plasma cells in lymphoid organs of OS patients, in which circulating B cells are undetectable. Hypomorphic *Rag2*^{R229Q} knock-in mice, which recapitulate OS, revealed, beyond severe B cell developmental arrest, a normal or even enlarged compartment of immunoglobulin-secreting cells (ISC). The size of this ISC compartment correlated with increased expression of Blimp1 and Xbp1, and these ISC were sustained by elevated levels of T cell derived homeostatic and effector cytokines. The detection of high affinity pathogenic autoantibodies toward target organs indicated defaults in B cell selection and tolerance induction. We hypothesize that impaired B cell receptor (BCR) editing and a serum B cell activating factor (BAFF) abundance might contribute toward the development of a pathogenic B cell repertoire in hypomorphic *Rag2*^{R229Q} knock-in mice. BAFF-R blockade reduced serum levels of nucleic acid-specific autoantibodies and significantly ameliorated inflammatory tissue damage. These findings highlight a role for B cells in OS pathogenesis.

CORRESPONDENCE
Anna Villa:
anna.villa@itb.cnr.it

Abbreviations used: CRC, clonally related cell; CSR, class switch recombination; FO, follicular; GC, germinal center; IFA, immunofluorescence; ISC, Ig-secreting cell; MZ, marginal zone; OS, Omenn syndrome; PD-1, programmed death-1; SCID, severe combined immunodeficiency.

Omenn syndrome (OS) is an inherited disorder characterized by the paradoxical coexistence of immunodeficiency and autoimmunity. OS is a genetically heterogeneous condition caused by a variety of genetic defects impairing lymphocyte development (Villa et al., 2008). Affected patients manifest with symptoms of severe combined immunodeficiency (SCID), including an increased occurrence of life-threatening infections, failure to thrive, and, in particular, autoimmune-like clinical features including early-onset severe erythrodermia, alopecia, hepato-splenomegaly, and lymphadenopathy (Omenn, 1965; Ochs et al., 1974). The best-characterized defects leading to OS are hypomorphic mutations in *RAG* genes, the first

E. Traggiai and A. Villa contributed equally to this paper.

© 2010 Cassani et al. This article is distributed under the terms of an Attribution–Noncommercial–Share Alike–No Mirror Sites license for the first six months–after the publication date (see http://www.rupress.org/terms). After six months it is available under a Creative Commons License (Attribution–Noncommercial–Share Alike 3.0 Unported license, as described at http://creativecommons.org/licenses/by-nc-sa/3.0/).

The Rockefeller University Press $30.00
J. Exp. Med.
www.jem.org/cgi/doi/10.1084/jem.20091928

The Journal of Experimental Medicine

Downloaded from jem.rupress.org on June 19, 2010

players in V(D)J recombination (Villa et al., 1998, 1999). The hallmark of OS, as a consequence of residual recombinase activity, is a peculiar immune phenotype made up of normal or elevated numbers of activated yet poorly functional T cells, with a highly restricted oligoclonal TCR repertoire. Such T cells infiltrate various organs, including skin, gut, spleen, and liver, resulting in profound tissue damage (Harville et al., 1997; Rieux-Laucat et al., 1998; Signorini et al., 1999). More recently, we and others have reported hypomorphic *Rag* mouse mutants that mimic many features of human OS (Khiong et al., 2007; Marrella et al., 2007); the study of these mice has led to a better understanding of the complexity of OS pathogenesis. Together, these models have clearly demonstrated that, in lymphopenic conditions, abnormal compensatory peripheral T cell proliferation and reduced thymic output could favor the expansion of T cell clones with inappropriate self-reactivity, and predispose to the development of immunopathology. Moreover, the lack of thymic *Aire* expression and the markedly reduced number of Foxp3$^+$ regulatory T cells suggested that impairment in both central and peripheral mechanisms of tolerance may contribute toward the development of autoimmunity both in mice (Marrella et al., 2007) and in humans (Poliani et al., 2009; Cassani et al., 2010).

In contrast, the B cell defect still remains one puzzling aspect of OS. Most of the OS patients have high IgE and residual IgG and/or IgM serum levels, though are virtually devoid of circulating B cells. On the other hand, later studies have shown that hypomorphic *RAG* mutations can, indeed, be associated with milder B cell phenotypes and, in such cases, Ig may be variably present (Villa et al., 2001; Sobacchi et al., 2006). The basis for this broad clinical spectrum is largely unknown, but epigenetic and environmental factors may play a causative role. Consistent with these observations, spontaneous hypomorphic *Rag1* mutant mice showed high serum levels not only of IgE but also of IgG and IgM isotypes. In the periphery, partial B cell maturation occurred, displaying a restricted BCR repertoire. Moreover, B cells in these mice responded to antigen challenge and T cell help, in agreement with the presence of functional germinal centers (GCs; Khiong et al., 2007). In contrast to the leaky B cell defect in this murine model, B cell differentiation seemed more heavily affected in *Rag2*^{R229Q} mice, similar to patients with typical OS (Noordzij et al., 2002). Indeed, a severe arrest at the pro–B stage was evident in the BM and was associated to a dearth of mature functional B lymphocytes in the peripheral lymphoid organs, which are depleted of B cell follicles (Marrella et al., 2007). Analogous to archetypal OS, the origin of elevated serum IgE levels in these mice remains to be elucidated.

Several lines of evidence led us to hypothesize that defects in RAG-mediated Ig gene editing/revision, either in the BM or in peripheral lymphoid tissues, might contribute to the development of the autoimmune phenotype (Hillion et al., 2005; Wang and Diamond, 2008). In addition to genetic susceptibility, autoreactive B cells can arise from the inability of a defective immune response to eradicate environmental pathogens. This results in a compensatory, often exaggerated chronic inflammatory response, ultimately leading to tissue damage and autoimmunity (Münz et al., 2009). Such a process may be favored in OS patients, in part because of defaults in the cellular and molecular components responsible for keeping inflammation in check (Villa et al., 2008).

Here, we have investigated the central and peripheral development of B cells in *Rag2*^{R229Q} mice, their function, as well as their contribution to the OS immunopathology. Our results show that in the presence of a severe BM B cell developmental defect, homeostatic and effector cytokines sustain the peripheral expansion of a few "nonconventional" mature, activated B cells, which engender a relatively increased compartment of Ig-secreting cells (ISCs). The resulting peripheral B cells are responsive to TLR agonists and T cell–independent antigens. We demonstrate that sera from *Rag2*^{R229Q} mice contain high-affinity anti-dsDNA and tissue-specific autoantibodies. *Rag2*^{R229Q} B cells display impaired receptor editing, and mutant mice have increased serum BAFF levels. Notably, BAFF-mediated rescue of autoreactive B cell clones was prevented by selective BAFF-R blockade, resulting in significant amelioration of tissue damage. Collectively, these findings point to an as yet unrecognized role of B cells in the OS immunopathology.

RESULTS

Detection of plasma cells in lymphoid organs of OS patients

OS patients are characterized by oligoclonal T cells, although they are virtually devoid of circulating B cells (Fig. 1 A and Table S1). However, high IgE and residual IgG and/or IgM serum levels indicate that Ig-producing plasma cells are actively present. Histological analysis of LN biopsies from two OS patients revealed a severe alteration of the microscopic architecture of the organ characterized by expansion of the paracortical area, along with severe depletion of the lymphoid cell population and lack of B cell follicles (Fig. 1 B, top left). Late B cell differentiation stages, including plasma cells and a subset of GC B cells, which are committed to plasma cell differentiation (Angelin-Duclos et al., 2000), are characterized by the expression of both Blimp1 and CD138, or Blimp1 alone, respectively. Accordingly, LN biopsies from healthy donors revealed the presence of a relatively small number of Blimp1$^+$CD138$^-$ late GC B cells, as well as Blimp1$^+$CD138$^+$ terminally differentiated plasma cells (Fig. 1 B, top right and inset). We detected Blimp1$^+$CD138$^+$ double-positive cells in both LN biopsies from OS patients, albeit at different levels (Fig. 1 B, bottom left and right). However, in contrast to LNs from healthy donors, Blimp1$^+$CD138$^-$ cells were only occasionally detected (unpublished data). Thus, in LNs from OS patients with undetectable circulating B cells, the large majority of Blimp1$^+$ cells represent an advanced stage of plasma cell differentiation.

We analyzed BM samples from four OS patients bearing RAG mutations for B cell subset composition. As expected from the recombinase defect, a severe block in B cell differentiation was evident, and mature B cells were barely detectable (Fig. 1 C). To better characterize this developmental arrest, we

Downloaded from jem.rupress.org on June 19, 2010

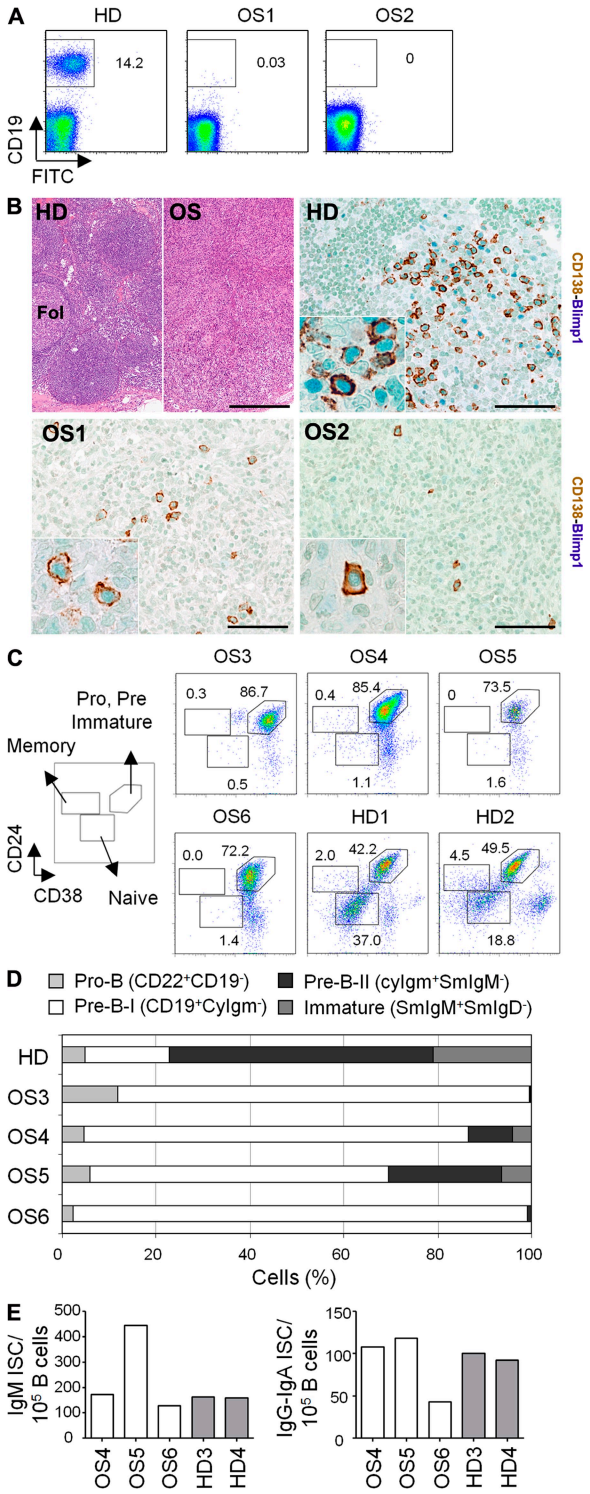

Figure 1. Analysis of the B cell compartment in OS patients. (A) Peripheral blood mononuclear cells were stained with anti-CD19 mAb and analyzed by flow cytometry in two independent experiments. FACS plots of one representative age-matched healthy donor (HD) and two OS patients with *RAG* mutations are shown. Numbers indicate percentage of cells. (B) Representative LN biopsies from HD and two OS patients have been stained by H&E and double immunostained with anti-CD138 and Blimp1. Bars: (top left) 200 µM; (top right and bottom left and right) 100 µM. (C) BM-derived mononuclear cells from patients and healthy donors were stained with anti-CD19, -CD24, and -CD38 mAbs. FACS plots shown are gated on CD19+ cells. Numbers indicate percentage of cells for each subset. (D) Composition of the precursor B cell compartment in OS patients ($n = 4$) compared with age-matched healthy children ($n = 9$). The BM precursor B cell compartment was set at 100% after exclusion of CD10−/SmIgM+/SmIgD+ mature B cells. (E) Frequency of ISCs in cultures of IgM and IgG-IgA isotypes. The number of spots/10^5 CD19+ B cells is reported. ELISpot analysis was performed once in two independent experiments.

used the differential expression of marker molecules to define various stages of B cell differentiation (van Zelm et al., 2005). In the BM from age-matched healthy children, ~18% of the precursor B cell compartment consisted of cytoplasmic (Cy) Igμ− cells, whereas in BM from all analyzed OS patients, ~92% (82–98%) of the precursor B cell compartment had this phenotype (Fig. 1 D). Interestingly, some CyIgμ+ pre–B-II cells and surface membrane (Sm) IgM+ immature B cells could be detected in patients OS4 and OS5 (Fig. 1 D). The mature B cell population (CD19+ SmIgM+ SmIgD+) was dramatically reduced in patients (<0.6% vs. 24% in healthy controls; unpublished data). However, ELISpot analysis revealed the presence of ISCs in the BM of all OS patients, producing either IgM or IgG/A (Fig. 1 E).

Characterization of BM and splenic B cell compartment in *Rag2*^{R229Q} mice

Given the obvious limitation in performing experiments with tissue samples from OS patients, we addressed the role of B cells in the pathogenesis of *Rag2*^{R229Q} mice, which recapitulate the main immune system alterations observed in OS patients (Marrella et al., 2007). Indeed, similarly to the majority of patients, *Rag2*^{R229Q} mice showed absent or dramatically reduced numbers of circulating B cells (Fig. 2 A), which is indicative of arrested B cell development. In the BM, *Rag2*^{R229Q} mice had a significantly reduced absolute number and percentage of B220+ B cells ($P < 0.0001$; Fig. 2 B and Fig. S1 A). Analysis of early B cell subsets showed a severe block in B cell differentiation at the pro–B cell stage, as indicated by the selective increase of early pro–B cells (B220+CD43+IgM− HSA^{low}BP-1−; Hardy et al., 1991; $P = 0.03$; Fig. S1 A and not depicted) and the severely reduced pre–B cells (B220+ CD43−IgM−), as well as IgM+IgD− immature B cells ($P < 0.0001$; Fig. 2 B and Fig. S1 A). As a consequence, the absolute number and relative proportion of splenic B220+ B cells were profoundly reduced in *Rag2*^{R229Q} mice ($P < 0.0001$; Fig. 2, C and D, and Fig. S1, B and C), with the complete absence of conventional transitional (T1 and T2) and mature B cells (Fig. 2 C and Fig. S1 B). The peripheral B cell pool was mainly composed of IgM+IgD− B cells, half of which expressed B220 (43.8 ± 12.3%; Fig. 2 C, bottom), and were negative for the AA4.1 and CD138 markers (not depicted). Notably, the expression of several cell activation markers (CD40, CD69, CD86, and MHC II) was augmented in B220+IgM+ cells from *Rag2*^{R229Q} mice when compared with the same subset from WT littermates

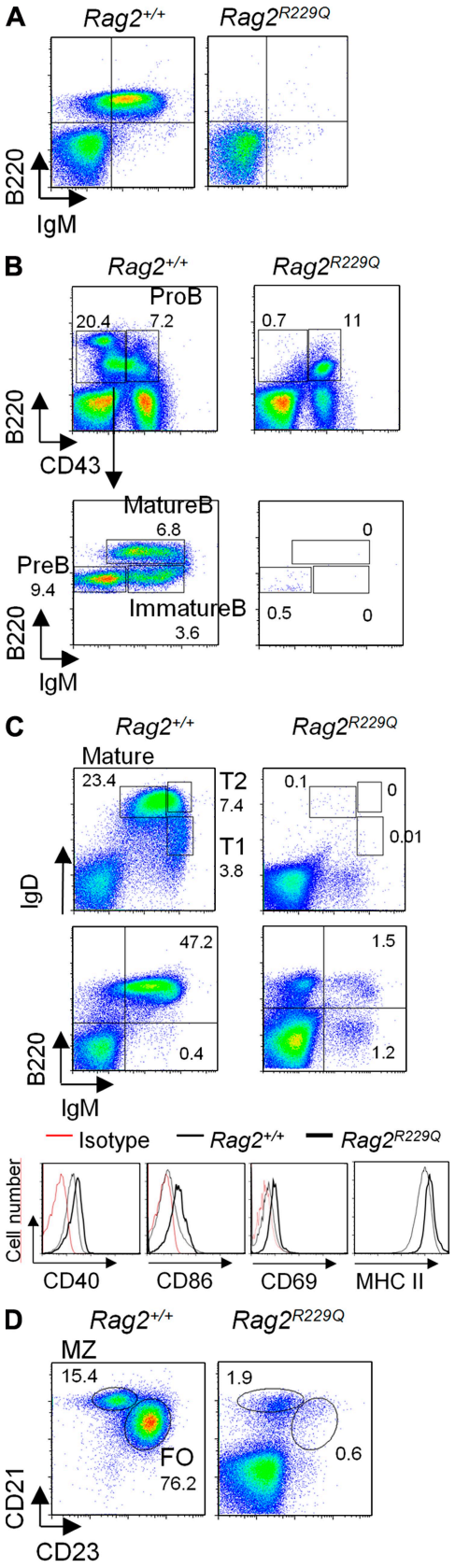

Figure 2. Characterization of the B cell compartment in *Rag2*^{R229Q} mice. (A) Analysis of circulating B cells from WT and *Rag2*^{R229Q} mice. (B) Total BM cells were labeled with anti-B220, CD43, IgM, and IgD to determine B cell developmental stages. Representative FACS plots are shown for mice (WT = 35 and *Rag2*^{R229Q} = 42) analyzed in six independent experiments. Numbers indicate percentage of cells for each gate. (C) Dot plots show analysis of splenic mature and transitional B cell populations from WT and *Rag2*^{R229Q} mice, using IgD and IgM markers. Histograms show expression of CD40, CD86, CD69, and MHCII activation markers in gated splenic B220$^+$ IgM$^+$ cells. Numbers indicate percentage of cells for each gate. (D) Splenocytes were labeled with anti-B220, -CD21, and -CD23 and analyzed by flow cytometry. Dot plots are gated on B220$^+$ cells. Numbers indicate percentage of cells for each gate. The results shown are representative of mice (WT = 43 and *Rag2*^{R229Q} = 57) analyzed in six independent experiments.

(Fig. 2 C). Among IgM$^+$ B cells, the mature naive splenic B cell compartment is made up of two populations designed as follicular (FO) B cells (B220$^+$CD23^{high}CD21^{low}) and marginal zone (MZ) B cells (B220$^+$CD23^{low}CD21^{high}). *Rag2*^{R229Q} mice had barely detectable IgM$^+$ MZ B cells and lacked mature IgD$^+$ FO B cells (Fig. 2 D and Fig. S1 C), consistent with the almost complete disruption of both MZ and FO organization (not depicted). In contrast, a CD21$^-$CD23$^-$B220$^+$ lymphocyte population was overrepresented in the mutant mice in comparison with WT littermates ($P = 0.0037$; Fig. S1 C). The CD21$^-$CD23$^-$ cells were CD43$^{-/low}$CD5$^-$Mac-1$^-$ and negative for sIg (not depicted), thus excluding the conventional B-1 lineage. These findings collectively suggest that in *Rag2*^{R229Q} mice some B cells may overcome the developmental block and colonize the periphery.

The presence of peripheral B cells in *Rag2*^{R229Q} mice prompted us to analyze the IgH repertoire. To this end, we cloned and sequenced the cDNAs encoding the Ig heavy chain (IgH) variable domain of IgM from bulk sorted B220$^+$ splenocytes (Table S2). The analysis of these sequences showed one dominant set of clonally related cells (CRCs) in each of the mutant mice, whereas we found only four small CRC clusters in the WT animal (Fig. S2 A). We additionally performed single-cell PCRs on individually sorted B220$^+$CD19$^+$ splenocytes of WT and *Rag2*^{R229Q} mice. Again, although we could not find CRCs in the normal mice, two out of three *Rag2*^{R229Q} animals showed CRC clusters (Fig. S2 A). The absence of CRCs from *Rag2*^{R229Q} B220$^+$CD19$^+$ B cells in the third sorting experiment is likely caused by the small number of sequences analyzed. Although we could not definitely demonstrate that *Rag2*^{R229Q} mice display a restricted Igh-V repertoire (Fig. S2 B), the results from single-cell PCR show expansion of a few CRCs in *Rag2*^{R229Q} mice.

ISC expansion in secondary lymphoid organs of *Rag2*^{R229Q} mice

With high variability, the production of serum IgG$_1$, IgG$_2$, and IgM was preserved in *Rag2*^{R229Q} mice (aged 1–9 mo), whereas IgG$_3$ and IgA were reduced ($P < 0.0001$; Fig. 3 A). Consistent with the OS phenotype, IgE levels were significantly higher in mutant mice ($P < 0.0001$). Thus, *Rag2*^{R229Q} mice are able to produce serum Ig of all isotypes, in spite of

Downloaded from jem.rupress.org on June 19, 2010

the apparent lack of mature B cells. To clarify this apparent discrepancy, we enumerated ISCs in cell suspensions derived from BM, spleen, and LNs by ELISpot. Using this analysis, we found a greater proportion of ISCs in secondary lymphoid organs of all *Rag2*^{R229Q} mice assayed compared with WT mice (Fig. S3 A). More pronounced differences were scored when ISC counts were normalized to B cell numbers. Indeed, mutant mice displayed 6–165-fold increases in IgM-, IgG-, IgA-, and IgE-secreting cells within the B cell compartment of spleen and LNs, compared with WT littermates (IgM, IgG, IgA, P = 0.008; IgE, P = 0.028; Fig. 3 B). In contrast, in the *Rag2*^{R229Q} BM, ISCs were retrieved to a lesser extent and with higher variability (Fig. 3 B). This observation correlated with the reduced expression of CXCL12 in *Rag2*^{R229Q} BM, the chemokine required for plasma cells homing and survival in BM niches (Tokoyoda et al., 2004; Fig. S3 B). These data revealed a larger expansion of the ISC population in *Rag2*^{R229Q} mice, mainly within the secondary lymphoid organs.

Plasmacytic differentiation is sustained by a program of gene expression, of which Blimp1 is considered to be the primary trigger (Martins and Calame, 2008). By quantitative PCR, we found that expression of Blimp1 is increased by threefold in splenic B220$^+$ B cells isolated from mutant mice as compared with controls (P = 0.029; Fig. 3 C). Increased Blimp1 expression also resulted in the induction of Xbp1, which is required for antibody production and secretion (Reimold et al., 2001; P = 0.029; Fig. 3 C). Differentiation to ISC with Blimp1 upregulation is associated with transcriptional repression of Bcl6 and c-Myc, characteristic of GC B cells (Lin et al., 1997; Shaffer et al., 2000). Accordingly, these transcripts were significantly reduced in *Rag2*^{R229Q} B220$^+$ cells (P = 0.029; Fig. 3 C). Therefore, although partially limited by the heterogeneity of the sorted B220$^+$ cell pool, these findings suggest that splenic B cells from *Rag2*^{R229Q} mice might have progressed further through a plasmacytic differentiation pathway than those of WT mice. Accordingly, in mutant mice, Xbp1 and Blimp1 expression were further increased in B220$^-$IgM$^+$ B cells with respect to B220$^+$IgM$^+$ B cells, indicative of an advanced stage of plasma cell differentiation (unpublished data). Furthermore, *Rag2*^{R229Q} B220$^+$ cells retained increased expression of Aid (P = 0.029; Fig. 3 C), which is essential for somatic hypermutation and isotype switching/class switch recombination (CSR).

Activated effector/memory T lymphocytes sustain ISC expansion, but do not help an antigen-specific response in *Rag2*^{R229Q} mice

B cell activation and plasmacytic differentiation might be cooperatively sustained by T cell activation. In *Rag2*^{R229Q} mice, CD4$^+$ T cells were skewed toward T_H-1 polarization, as indicated by increased production of IFN-γ, but not of IL-4 and IL-10 cytokines upon PMA/ionomycin stimulation (Fig. 4 A). Interestingly, CD4$^+$ T cells from *Rag2*^{R229Q} mice had a substantially increased percentage of IL-17–producing cells (Fig. 4 A). Accordingly, *Rag2*^{R229Q} CD4$^+$ T cells displayed significantly increased mRNA levels for the Th1-specific T-bet transcription factor and reduced mRNA levels for GATA-3, which directs Th2 polarization (P = 0.03; Fig. 4 D; Szabo et al., 2002). Significantly higher mRNA levels for the Th17-specific RORγt transcript were also detected. Thus, Th1 and Th17 cells could be implicated in the inflammatory condition characteristic of *Rag2*^{R229Q} mice.

Th17 cells secrete large amounts of IL-21, which then acts to amplify the

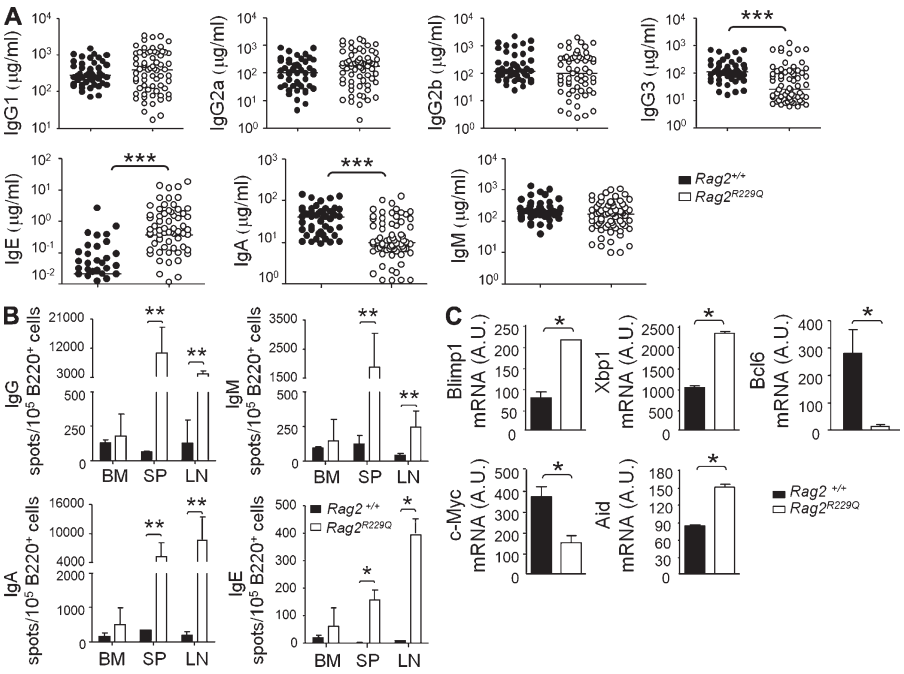

Figure 3. Serum Ig levels and ISC in lymphoid organs. (A) Sera from naive WT (*n* = 49) and *Rag2*^{R229Q} (*n* = 67) mice (5–37 wk-old) were collected and their IgG1, IgG2a, IgG2b, IgG3, IgM, and IgA concentrations were determined by luminex technique using a Bioplex reader. Each serum sample was run in duplicate, and five independent assays were performed. Serum IgE concentrations were measured by ELISA in five independent experiments. (B) The frequency of IgM-, IgG-, IgE-, and IgA-secreting cells in the BM, spleen, and LNs of naive WT and *Rag2*^{R229Q} mice (10–12 wk old) was determined by ELISpot. The number of spots/10^5 B220$^+$ cells is indicated. Results are mean ± SD of five independent experiments testing a total of 17 mice/group. (C) Transcriptional programming sustains ISC differentiation in *Rag2*^{R229Q} mice. B220$^+$ lymphocytes were purified by cell sorter from total splenocytes of WT (*n* = 6) and *Rag2*^{R229Q} mice (*n* = 12). Expression levels of different transcription factors were normalized to 18S rRNA. Quantitative RT-PCR was run in triplicates. Relative measures are indicated as arbitrary units (A.U.). Data represent one of the three independent experiments with consistent results. *, P < 0.05; **, P ≤ 0.01; ***, P ≤ 0.001.

Th17 response in an autocrine fashion (Korn et al., 2007; Zhou et al., 2007). Analysis of serum cytokines by ELISA revealed that mutant mice had elevated levels of IL-21 (P = 0.0113) and IFN-γ (P = 0.0007; Fig. 4 B). Because production of both IL-17 and IL-21 cytokines has been associated to FO helper T cells (T_{FH} cells; Bauquet et al., 2009; Chtanova et al., 2004), in addition to T_H-17 cells, we analyzed the CD4+ T cell subset for the expression of CXCR5 and ICOS, crucially involved in T_{FH} cells homing and differentiation (Schaerli et al., 2000; Mak et al., 2003). An increased proportion of ICOS+ cells was observed in *Rag2*^{R229Q} CD4+ splenocytes (41.6% vs. 7.7%; *n* = 6; P = 0.008), and more CD4+ ICOS^{hi} T cells expressed CXCR5 in *Rag2*^{R229Q} mice (7.7% vs. 1.5%; *n* = 6; P = 0.008; Fig. 4 C). *Rag2*^{R229Q} CD4+ CXCR5+ ICOS^{hi} T cells expressed WT levels of CD40L, but increased levels of programmed death-1 (PD-1; Fig. S4), both of which are co-stimulatory molecules necessary for T_{FH} cell generation and function (Vinuesa et al., 2005). The mRNA encoding the transcription factor Bcl6, a determinant of the T_{FH} cell fate (Nurieva et al., 2009), was also significantly increased in *Rag2*^{R229Q} CD4+ splenocytes (P = 0.03; Fig. 4 D). Overall, these data define subsets of T helper cells with the potential to activate B cells and promote their differentiation into ISC in *Rag2*^{R229Q} mice. To better clarify the T cell contribution to B cell phenotype in *Rag2*^{R229Q} mice, we treated mutant mice with the anti-CD4 mAb (GK1.5) for 7 wk. This treatment resulted in a complete depletion of circulating, splenic, and BM CD4+ T cells (Fig. 5 A). Concomitant to the depletion of CD4+ T cells, we observed a significant reduction of the frequency of IgG and IgA but not IgM-secreting cells in the spleen and BM of treated mice (Fig. 5 B), correlating with the serum Ig levels (Fig. 5 C). Anti-CD4 treatment determined a complete normalization of the IgE serum level in *Rag2*^{R229Q} mice (Fig. 5 C) and a substantial decrease in the concentrations of CSR-driving cytokines, IFN-γ and IL-21 (Fig. 5 D). Thus, these findings highlight the contribution of CD4+ T cells in sustaining B cell activation and plasma cell differentiation in *Rag2*^{R229Q} mice.

We next investigated whether *Rag2*^{R229Q} mice could mount a T cell–dependent immune response in vivo. Mutant and WT mice (10 wk of age) were immunized into the footpad with OVA in CFA and boosted with recall antigen in immunofluorescence (IFA) on day 21. At regular intervals, sera were analyzed simultaneously for total and OVA-specific antibodies. As expected, in normal mice immunization resulted in a rapid and significant increase of total IgG serum levels (P = 0.03; Fig. 6 A and not depicted), whereas no IgG elevation was observed in *Rag2*^{R229Q} mice (Fig. 6 A). Moreover, in WT animals OVA-specific IgG levels were detectable immediately after the boost and sustained after 48 d (Fig. 6 B). In contrast, we could not detect a secondary anti-OVA IgG response in the sera from *Rag2*^{R229Q} mice (Fig. 6 B). These results were matched by the analysis of the frequency of antigen-specific ISC as measured by ELISpot. Unimmunized *Rag2*^{R229Q} mice made significantly more IgG-secreting cells than WT mice (P = 0.008; Fig. 6 C). However, after boosting, an increased number of IgG plasma cells were detectable exclusively in the spleens of WT mice (P = 0.029) from days 26 to 33, and returned to nearly baseline levels by day 48, which is consistent with the IgG serum levels (Fig. 6 C). A similar trend was observed in the response of WT mice using the ELISpot assay (Fig. 6 D). No OVA-specific IgG-secreting cells could be detected in the *Rag2*^{R229Q} mice at any of the time points assayed (Fig. 6 D), indicating

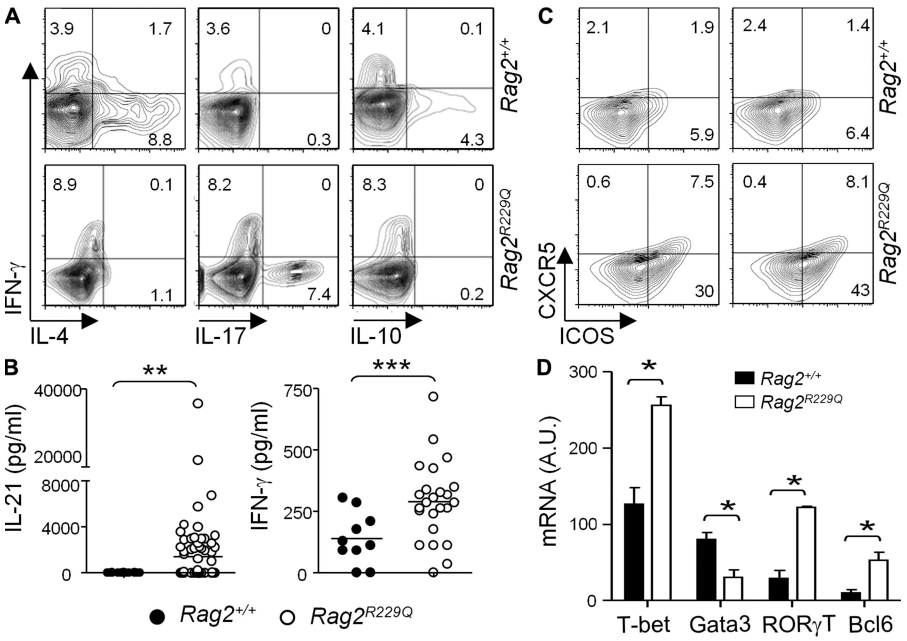

Figure 4. Characterization of effector T cell subsets in *Rag2*^{R229Q} mice. (A) Cytokine production profile of splenic CD4+ T cells. Total splenocytes were stimulated for a total of 5 h in the presence of PMA and ionomycin. Cytokine production was assessed by flow cytometry with intracellular staining. Plots are gated on CD4+ T cells. Numbers indicate the percentage of cells in the respective quadrants. Data represent one of the three independent experiments with consistent results. (B) Serum levels of IL-21 (WT, *n* = 30; *Rag2*^{R229Q}, *n* = 50) and IFN-γ (WT, *n* = 30; *Rag2*^{R229Q}, *n* = 50) cytokines in WT and *Rag2*^{R229Q} mice (8–24 wk old) as analyzed by ELISA in three independent experiments. (C) Expression of CXCR5 and ICOS by CD4+ splenic T cells from WT and *Rag2*^{R229Q} mice. Numbers in quadrants indicate percentage of cells in each. (D) Expression of indicated molecules in sorted splenic CD4+ T cell population assessed by qRT-PCR. Samples were run in duplicate, and the target mRNA was normalized to *Ppia* mRNA. The RNA contents are shown as arbitrary units (A.U.). Means ± SD of six mice/group. Data represent one of the three independent experiments with consistent results. *, P < 0.05; **, P ≤ 0.01; ***, P ≤ 0.001.

Published June 14, 2010

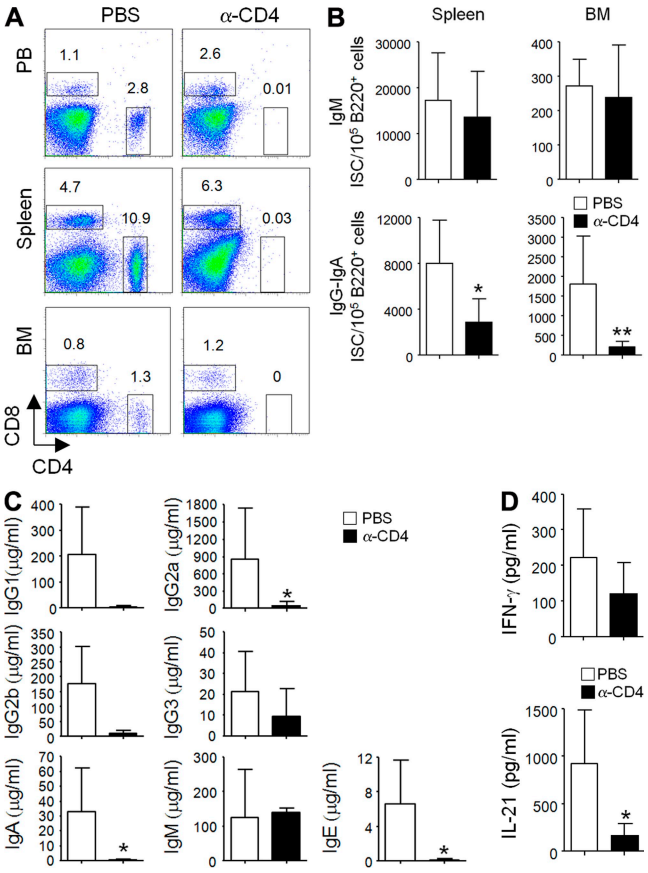

Figure 5. CD4 T cells sustain ISC differentiation in *Rag2*^{R229Q} mice. *Rag2*^{R229Q} mice (5 wk-old) were injected i.v. with two doses of anti-CD4 mAb (0.25 mg/mouse) 3 wk apart and were analyzed after 7 wk. (A) Representative FACS plots of CD4 and CD8 stainings in treated mice and controls. (B) ISC by ELISpot assay. Data represent the mean ± SD number of spots obtained from n = 5–6 mice/group analyzed and normalized to 10^5 B220$^+$ cells. Serum Ig (C) and cytokine (D) levels in treated and control mice. Data represent the mean ± SD of concentrations observed in n = 5–6 mice/group analyzed. *, $P < 0.05$; **, $P \leq 0.01$.

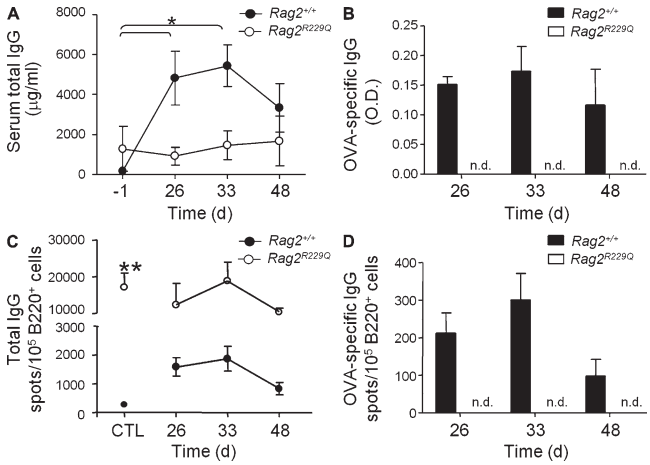

Figure 6. *Rag2*^{R229Q} mice fail to induce specific humoral response to OVA. WT and *Rag2*^{R229Q} mice were immunized into the footpad with OVA emulsified in CFA and boosted at day 21 in IFA. PBS was injected in control mice. Total IgG1 (A) and anti-OVA–specific IgG (B) antibody titers were determined at days 26, 33, and 48 after challenge by ELISA. Each point represents mean values + SD from n = 3–4 mice and were corrected for background binding. Frequency analysis of total (C) and specific (D) ISCs by ELISpot assay on splenocytes from WT and *Rag2*^{R229Q} mice at the indicated times after OVA challenge. Data represent the mean ± SD number of spots obtained from n = 3–4 mice/group analyzed in two independent experiments and normalized to 10^5 B220$^+$ cells. n.d., not detectable. CTL, PBS-treated control mice. *, $P < 0.05$; **, $P \leq 0.01$.

that the observed absence in IgG production resulted from an impaired generation of specific antibody-secreting cells.

Humoral response to TLR agonists and T cell–independent antigen in *Rag2*^{R229Q} mice

It is well established that Toll-like receptor (TLR)–mediated activation of mature B cells is required for eliciting humoral immune responses (Pasare and Medzhitov, 2005). Mature murine B cells can be stimulated in vitro by LPS or CpG (the TLR4 and TLR9 ligand, respectively) to proliferate and secrete antibodies (Watson, 1979; Krieg et al., 1995). We evaluated the expression of TLR4 and TLR9 by real-time PCR in purified *Rag2*^{R229Q} B220$^+$ cells, and found a reduction in comparison to WT cells (Fig. 7 A). Moreover, *Rag2*^{R229Q} B220$^+$ cells did not cycle in response to LPS or CpG and IL-4 co-stimulation (Fig. 7 B). Because proper interpretation of these results could be hindered by the heterogeneity of the B220$^+$ cell subset, we also evaluated the Ig production. Analysis of Ig in the supernatants at day 4 of culture indicated that mutant B cells were able to switch and secrete Ig at a rate comparable to control B cells, and particularly upon CpG stimulation (Fig. 7 C). To confirm in vivo the T cell–independent humoral responsiveness of *Rag2*^{R229Q} B cells, we immunized mutant mice i.p. with a mixture of pneumococcal antigens (Pneumovax23-P23) and monitored total and specific IgM serum antibodies at different time points after immunization (from day 10 to 60). The increase in total and specific serum IgM was lower in *Rag2*^{R229Q} with respect to WT littermates (Fig. 8, A and B). However, in the *Rag2*^{R229Q} B220$^+$ population we detected a higher frequency of ISC secreting P23-specific IgM which decayed rapidly (Fig. S5, C and D). The possible homing of specific ISC in the BM was excluded by the failure to detect P23-specific ISC in the BM of mutant mice (unpublished data). The apparent discrepancy between ELISpot results and serum titers could be explained by considering the markedly reduced size of the splenic B cell compartment in mutant mice. Low absolute numbers of P23-specific IgM ISC would be unable to determine WT antibody titers. Moreover, *Rag2*^{R229Q} displayed a more rapid decrease in specific serum antibodies reaching the pre-boost level at day 20, indicating a selective impairment in the generation of long-term humoral responses (Fig. 8, A and B). Collectively, our results show that *Rag2*^{R229Q} mice are able to mount short-term specific humoral immune responses, which do not require T cell help for their generation.

Downloaded from jem.rupress.org on June 19, 2010

Published June 14, 2010

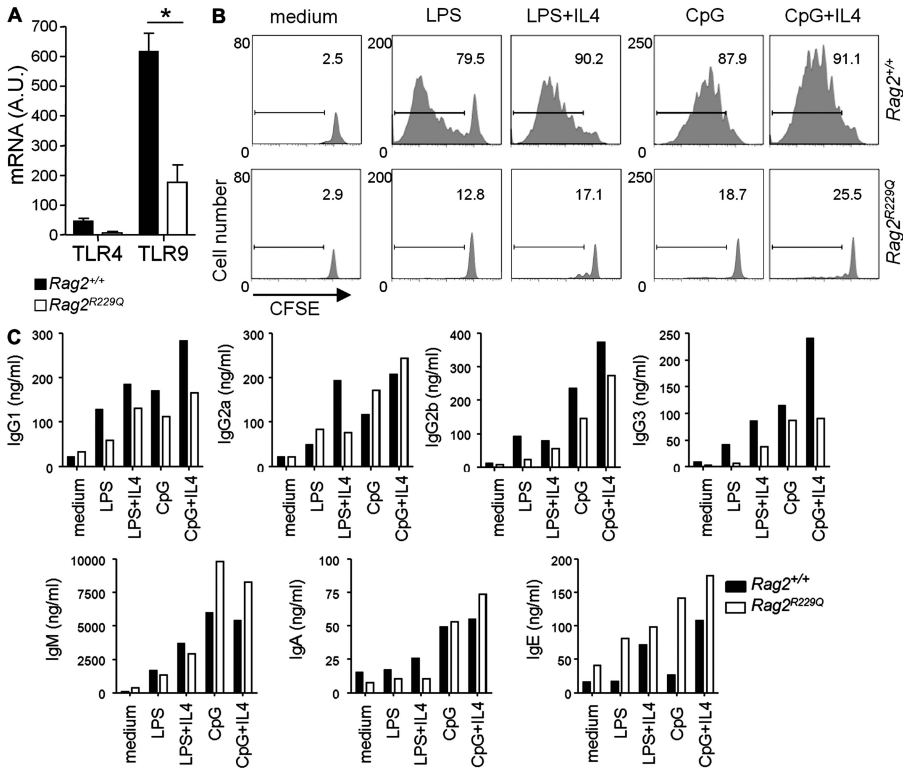

Figure 7. *Rag2*^{R229Q} mice have impaired proliferative responses to TLR agonists but intact Ig responses. (A) Splenic B220$^+$ lymphocytes were purified by cell sorting, and the relative mRNA levels of TLR4 and TLR9 expression were determined by RT-PCR. The samples were run in duplicates. The obtained values were normalized to 18S rRNA and indicated as arbitrary units (A.U.). Mean values ± SD of three independent experiments testing eight mice/group. (B) Total splenocytes were CFSE labeled, and then stimulated in vitro with LPS (10 µg/ml) and CpG (2.5 µg/ml) in the absence or presence of IL-4 (10 ng/ml). CFSE dilution was analyzed by FACS at day 4 of culture. Representative FACS histograms of CFSE profile in B220$^+$ cell gate are shown (percentage is reported above the gate). The histogram plot is representative of three independent experiments (C) In parallel, Ig levels were measured in the culture supernatants. Ig concentrations were normalized for the number of B220$^+$ cells in the culture. *, P < 0.05.

B cells from *Rag2*^{R229Q} mice actively participate to tissue damage

A proportion of *Rag2*^{R229Q} mice spontaneously develop severe alopecia, skin erythrodermia, and wasting syndrome caused by colitis (Marrella et al., 2007). In addition, a minority of them presented with differing degrees of renal damage, resulting in proteinuria. A marked infiltration of oligoclonal activated T lymphocytes was consistently evident in different tissues of mutant mice and correlated with abnormal CXCL10 serum level (P = 0.002; Fig. S6 A). Further characterization of these infiltrates revealed that they were also composed of B220$^+$ Ig$^+$ B cells (Fig. 9 A; Fig. S6, B and C). The abundance of B220$^+$ and IgM$^+$ cell infiltrates was lower with respect to CD3$^+$ T cells (P = 0.048 and P = 0.0098, respectively; Fig. S6 C), which may reflect the absence of circulating B cells, as well as the significantly lower representation of B lymphocytes in primary and secondary lymphoid organs of *Rag2*^{R229Q} mice. Nonetheless, a direct role of B cells in the disease pathogenesis was suggested by the severe glomerulus infiltration of IgM$^+$ and IgG$^+$ cells (Fig. 9 A, top) in mice with high proteinuria index, whereas no tissue infiltration was observed in nonproteinuric mice (Fig. 9 A, bottom). To further investigate whether autoantibody production might contribute to the autoimmune phenotype, we screened a large cohort of *Rag2*^{R229Q} and control animals for the presence of anti–double-stranded DNA (anti-dsDNA) measured by ELISA and IFA with *Chionodoxa luciliae*, two complementary assays for detection of DNA autoantibodies characterized by low and high specificity, respectively. We observed a significant increase in the frequency of sera positive for both IgG and IgM specific for dsDNA in the group of mutant mice as compared with WT (P < 0.01; Fig. 9 B and not depicted). Notably, high titers of IgG anti-dsDNA were detected in animals with severe kidney infiltrations and urine protein loss (unpublished data). Staining of frozen sections of multiple organs from *Rag2/Il2rc* double knock-out mice (devoid of endogenous Ig) with sera derived from mutant mice confirmed the presence of autoreactive Ig targeting different tissues (Fig. 9 C).

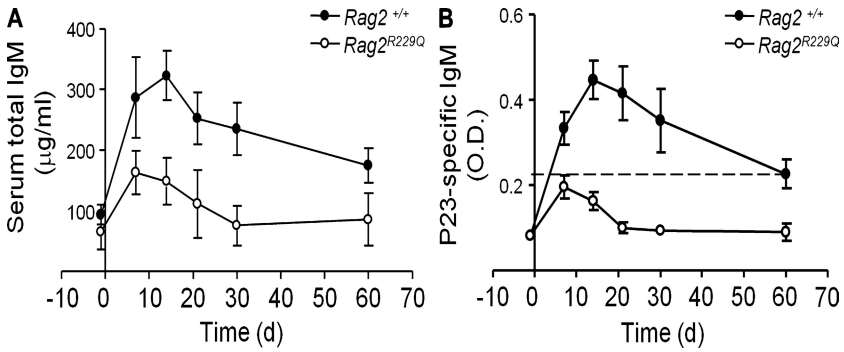

Figure 8. *Rag2*^{R229Q} mice show short-term humoral response to Pneumovax23. WT and *Rag2*^{R229Q} mice were immunized i.p. with P23. PBS was injected in control mice. Total (A) and anti-P23–specific IgM (B) antibody titers were determined at different days after challenge by ELISA. Each group represents mean values ± SD from *n* = 5 mice and were corrected for background binding. The data are representative of two independent experiments.

Downloaded from jem.rupress.org on June 19, 2010

These findings are indicative of defaults in B cell selection and tolerance. Receptor editing is the mechanism by which B lymphocytes alter their antigen receptors through secondary antibody gene rearrangements, usually involving the κ and λ light chain gene loci. Repeated variable joining rearrangements eventually lead to exhaustion of the recombination potential at the *Igk*-V gene locus and expression of a λ light chain. A markedly reduced frequency of λ chain$^+$ B220$^+$ cells was observed in mutant mice (1.5 ± 1% vs. 4.7 ± 1.6%; P = 0.0002; Fig. 9 D), thus suggesting that *Rag2*^{R229Q} mutation impairs the process of secondary recombination. In normal conditions, peripheral self-reactive B cells compete with non–self-reactive B cells for survival factors. BAFF is the key regulator of B cell homeostasis beyond the late transitional B cell stage (Meyer-Bahlburg et al., 2008), when expression of BAFF-R is acquired on B cells. Because increased BAFF levels are expected in mice with reduced B cell numbers (Lesley et al., 2004; Lavie et al., 2007), we measured BAFF serum levels in our model. Significantly, higher levels of BAFF were already detected in *Rag2*^{R229Q} mice (P < 0.0001; Fig. 9 E) early in life (5-wk-old animals), whereas in WT mice the increase in BAFF serum levels was age-dependent (Fig. S6 D).

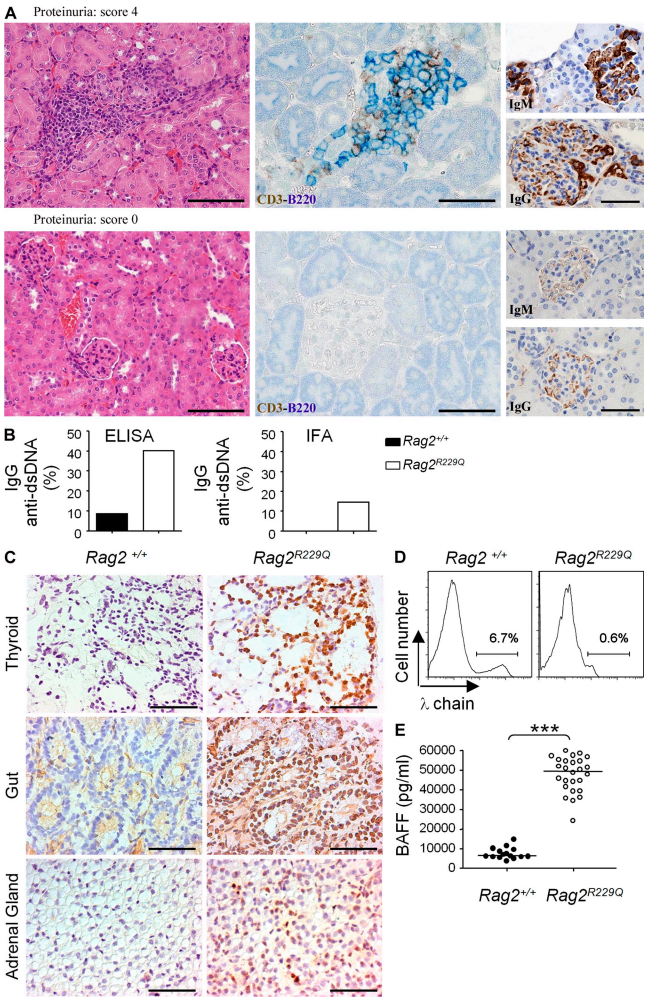

Figure 9. Residual autoreactive B cells in *Rag2*^{R229Q} mice contribute to tissue damage in autoimmune-like manifestations. (A) Characterization of kidney infiltrates and correlation with clinical symptoms. Kidney sections from a mouse with proteinuria (score 4: ≥ 2000 mg/dl; top) and a mouse without renal disease (bottom). Kidneys from mice with proteinuria show infiltrates positive for staining with CD3, B220, IgM and IgG. Bars: (left) 100 µM; (middle) 50 µM; (right) 60 µM. (B) The presence of IgG anti–double-strand DNA autoantibodies was analyzed in the sera of WT (*n* = 70) and *Rag2*^{R229Q} (*n* = 97) mice by ELISA and IFA in five independent experiments. Bars indicate the frequency of positive sera in mice aged 8–24 wk. (C) Ig targeting tissues are detected in the sera of *Rag2*^{R229Q} mice. Frozen sections obtained from, gut, thyroid, and adrenal gland of *Rag2/Il2rc* double-KO mice were incubated with sera obtained from WT and *Rag2*^{R229Q} mice. Staining with anti-mouse IgG Ab followed by incubation with secondary, anti-mouse IgG peroxidase-conjugated antibody was performed. Representative images from 1 out of 10 mice tested/group. Bars, 100 µM. (D) FACS analysis of λ light chain expression in gated B220$^+$ IgM$^+$ cells. Results are representative of 11 mice/group analyzed in three independent experiments. (E) Serum BAFF in *Rag2*^{R229Q} (*n* = 26) and WT littermates (*n* = 15), measured by ELISA in two independent experiments. **, P ≤ 0.01; ***, P ≤ 0.001.

Effect of BAFF-BAFF-R signaling blockade in *Rag2*^{R229Q} mice

As BAFF promotes B cell survival, its overexpression could potentially break B cell tolerance by rescuing self-reactive B cells from deletion. Indeed, mice transgenic for *Tnfsf13b* (the gene encoding BAFF) develop severe autoimmune symptoms (Mackay et al., 1999; Lesley et al., 2004; Thien et al., 2004). Based on this evidence, we speculated that increased BAFF serum levels in *Rag2*^{R229Q} mice could play a crucial role in B cell–mediated autoimmunity by favoring the survival and differentiation of autoreactive ISCs. To directly test this hypothesis, we examined the in vivo effect of selective BAFF-BAFF-R signaling blockade. Mutant mice displaying an overt pathological phenotype (i.e., presence of serum anti-dsDNA IgG and proteinuria) were i.v. injected with three 0.5-mg doses of anti–BAFF-R mAb (9B9) known to prevent BAFF binding (Rauch et al., 2009), and followed for 2 mo. *Rag2*^{R229Q} mice treated with anti–BAFF-R mAb showed a significant decrease in the number of splenic B220$^+$ B cells compared with PBS-treated (control) animals (P = 0.008; Fig. 10 A). In WT mice, administration of anti–BAFF-R resulted in 90% depletion of FO B cells and 68% depletion of MZ B cells (unpublished data). Interestingly, a marked reduction of both CD4 and CD8 T cells was observed in mutant, but not WT mice, consistent with the role of BAFF signaling on activated T cells (Mackay and Leung, 2006; unpublished data).

The frequency of IgM, IgG, and IgA-ISC in the spleen was not significantly different in treated versus control mutant mice, but because of the smaller splenic B cell counts, the total number of ISC was significantly lower in anti–BAFF-R–treated *Rag2*^{R229Q} mice than controls (P < 0.001; Fig. 10 B and not depicted). After euthanization, histological examinations were performed and the degree of cell infiltration was scored in different organs (liver, gut, lung, kidney, and skin). Remarkably, a significantly decreased infiltration index was generally observed in *Rag2*^{R229Q} anti–BAFF-R–treated mice

Published June 14, 2010

compared with controls, and specifically in the extent of infiltrating B220$^+$ and IgM$^+$ B cells (Fig. 10 C). The potential clinical effect of anti–BAFF-R administration was also evaluated. The *Rag2*^{R229Q} mice studied manifested similar proteinuria levels at the beginning of treatment, which significantly worsened over time in mice treated with PBS (P = 0.04; Fig. 10 D). In contrast, stabilization of kidney disease was observed in anti–BAFF-R–treated mice, with 4/7 mice displaying a reduction in the proteinuria index (Fig. 10 D). Consistently, the treated mice had markedly reduced signs of glomerular damage compared with the control mice that showed mesangial cell proliferation and heavy deposition of IgG (Fig. 10 D). Furthermore, 2 mo after treatment, the disappearance of IgG anti-dsDNA antibodies was detected in the majority of the treated mice (Fig. 10 D). Overall, these results support a causative role of B cells in the *Rag2*^{R229Q} immunopathology, providing preliminary evidence for a potential therapeutic application of BAFF-BAFF-R signaling blockade.

DISCUSSION

In this study, we have exploited *Rag2*^{R229Q} mice, which reproduce the immunopathology observed in OS patients, to address whether B cells play any role in the pathogenesis of the disease. The impairment of early B cell development in *Rag2*^{R229Q} mice determines a dramatic reduction of the peripheral B cell compartment, which is characterized by the presence of Ig-negative precursors and only a few IgM$^+$ IgD$^-$ B cells, which express several activation markers. FO B cells were almost undetectable, whereas splenic MZ B cells were barely present. In contrast, mutant animals contained an expanded CD21$^-$CD23$^-$IgM$^-$ lymphocyte population. This phenotype could be reminiscent of mice with defective B cell development caused by lack of the surrogate light chain. In fact, these mice displayed an expanded B220$^+$CD21$^-$CD23$^-$IgM^{low} cell subset and produced ANAs upon in vitro polyclonal stimulation (Harfst et al.,

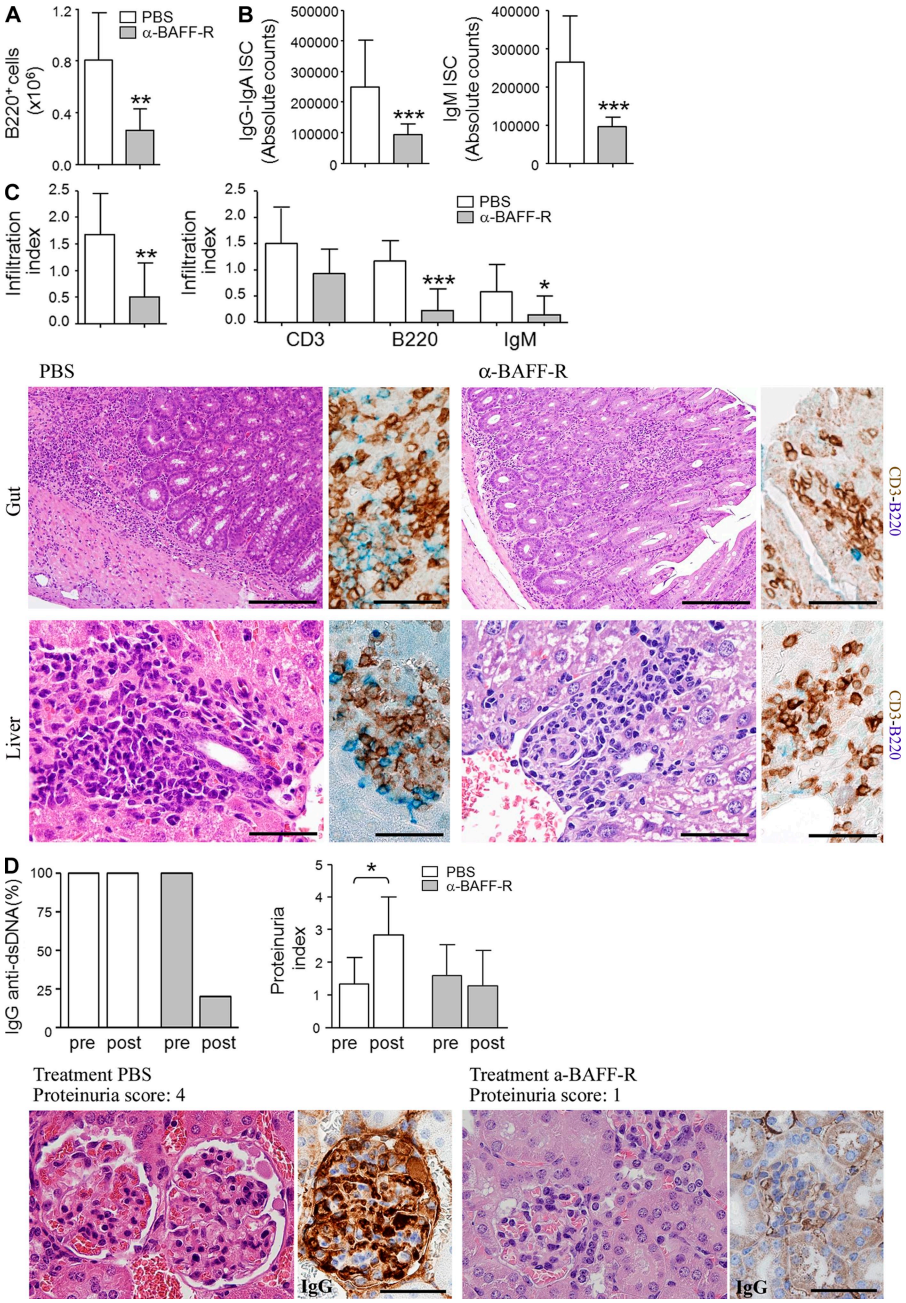

Figure 10. Effect of anti–BAFF-R mAb administration in *Rag2*^{R229Q} mice. Mutant mice were treated with three doses of 0.5 mg anti–BAFF-R mAb or PBS, and followed for a total period of 2 mo. (A) Splenic B220$^+$ cell counts. (B) Absolute numbers of splenic ISC. Mean values ± SD obtained from n = 6–7 mice/group. (C) The global and cell-specific (CD3$^+$, B220$^+$, IgM$^+$) degree of infiltration was scored in different organs (liver, kidney, lung, and gut) from anti–BAFF-R mAb and PBS-treated mice. Bars indicate the mean ± SD infiltration index calculated for all the organs from n = 6–7 mice/group. Images show immunostains of gut and liver from representative PBS and anti–BAFF-R mAb-treated mice. Bars: (left) 200 µM; (right) 50 µM. (D) The presence of high-affinity IgG anti-dsDNA autoantibodies was analyzed in the sera of PBS and anti–BAFF-R *Rag2*^{R229Q} mice by IFA, before and after the treatment. Bars indicate the frequency of positive sera. Proteinuria was assessed before and after treatment of *Rag2*^{R229Q} mice with PBS and anti–BAFF-R, respectively. Mean values ± SD of proteinuria index in n = 6–7 mice/group. (bottom) Representative images of glomeruli from untreated proteinuric mice and anti-BAFFR–treated mice. Bars, 50 µM.

Downloaded from jem.rupress.org on June 19, 2010

2005; Keenan et al., 2008). Based on this, it can be speculated that in *Rag2*^{R229Q} mice most of the peripheral B cells carry autoreactive potential.

The analysis of a large cohort of mutant mice revealed, in some animals, a normal or even higher Ig production compared with WT mice. This variability, resembling the clinical phenotype reported in OS patients (Villa et al., 2001), is actually greater than the one previously reported by Marrella et al. (Marrella et al., 2007). Such a discrepancy could likely reflect the mixed genetic background of our model and the effects of stochastic events occurring during B cell repertoire generation. In mutant mice, the residual serum Ig production is maintained by an enlarged ISC compartment. Excessive commitment to plasma cell fate is sustained by a defined transcription program. The observed increase in Blimp1 likely leads to cessation of cell cycling activity in *Rag2*^{R229Q} B cells (Lin et al., 1997), repression of genes required to establish GC reactions, and induction of the Ig secretory pathway (Shaffer et al., 2002; Shaffer et al., 2004). Our findings correlate with previous observations in immunodeficient and/or irradiated hosts, reconstituted with a limited number of peripheral B cells (Agenès and Freitas, 1999). In these animals, B cells quickly expanded, displayed an activated phenotype, and gave rise to an increased proportion of plasma cells. Hence, a compensatory homeostatic regulation might account for the skewed B cell phenotype in our model. During inflammation Aid and Blimp1 expression can be induced in immature/T1 B cells by TLR engagement in a T cell–independent manner (Ueda et al., 2007). Consistently, Aid^{+} immature/T1 B cells were preferentially found outside the conventional GC, at sites exposed to exogenous antigens (Wang et al., 2000; Ueda et al., 2007). The most severe inflammatory and autoimmune-like manifestations in *Rag2*^{R229Q} mice affect organs like the gut and the skin, where exposure to microbial antigens could potentially select immature B cell clones for expansion and antibody production. We showed that B cells from *Rag2*^{R229Q} mice efficiently responded to TLR ligands and polysaccharides Ag by undergoing rapid plasmacytic differentiation and Ig class switching. The limited variability consequent to impaired recombinase activity and the stochastic nature of B cell repertoire generation might represent factors determining the phenotypic heterogeneity of OS patients.

Several experiments in this study addressed the role of T cells in B cell homeostasis in *Rag2*^{R229Q} mice. We found that CD4 T cells were required for B cell activation and differentiation to plasmablasts in *Rag2*^{R229Q} mice. We provided evidence that the dominating T cell subsets in mutant mice, namely Th1, Th17, and T_{FH} cells do have a crucial role in B cell abnormalities. In fact, anti-CD4 treatment caused a significant reduction of ISC compartment and a normalization of serum IgE. These results correlated with the decreased serum concentration of cytokines involved in CSR such as IFN-γ and IL-21. Interestingly, IL-21 has recently been reported to stimulate IgE synthesis in humans, thus highlighting its important role in the occurrence of allergic and atopic disorders (Kobayashi et al., 2009). Furthermore, we demonstrated that T cell help for B cells was not dependent on cognate interaction, as *Rag2*^{R229Q} mice were severely impaired in the antibody response to TD antigens. The lack of OVA-specific IgG production might be caused by impaired T-B cell collaboration in the absence of GC-like structures. On the other hand, in this issue, Walter et al. show that adoptive transfer of WT CD4^{+} T lymphocytes was unable to correct defective antibody response to TNP-KLH, indicating B cell intrinsic abnormalities.

In *Rag2*^{R229Q} mice, a skewed pattern of cytokines expression and T helper cell bias may favor B cell–mediated autoimmunity. Dysregulated T_{FH} cells produce large amounts of IL-21, which promotes B cell activation as well as secretion of pathogenic anti-dsDNA autoantibodies and contributes to chronic T cell–mediated autoimmune inflammation by the generation of Th17 cells. Interestingly, it has been shown that IL-17 acts in synergy with BAFF in supporting B cell proliferation and differentiation to plasma cells in SLE patients (Hutloff et al., 2004; Iwai et al., 2003). In our model, homeostatically proliferating T cells are critical for the generation of ISCs, as well as the induction of the hyper-IgE state in mutant mice, and most likely contribute toward the pathogenesis of distinctive OS clinical features.

On the other hand, autoimmunity develops to the same extent in T cell–sufficient and T cell–deficient BAFF-transgenic mice (Groom et al., 2002), indicating that BAFF-mediated rescue of self-reactive B cells may be T cell independent. High-affinity anti-dsDNA serum IgG autoantibodies together with severe kidney damage with proteinuria, which we observed in *Rag2*^{R229Q} mice, are pathognomonic signs of B cell–mediated autoimmunity (Sobel et al., 1991; Manson et al., 2009). In the hypomorphic *Rag1* murine model described by Walter et al. (2010), only low-affinity IgG autoantibodies were detected and the majority of the mice were devoid of clinical symptoms. This variability in clinical phenotype may reflect the different impact of the genetic defect on the recombination activity and the contribution of environmental factors.

Fewer B cells expressing λ chain in the mutant mice is suggestive of defects in the secondary rearrangements (Vela et al., 2008). Because an impairment in this process would also affect autoreactive Ab-expressing B cells, which could not therefore be silenced by light chain editing, it can be speculated that hypomorphic *Rag2* mutation leading to impaired RAGs activity limits the potential to edit autoimmune BCRs. Under physiological conditions, self-reactive B cells that escape deletion and receptor editing, compete with nonautoreactive B cells for peripheral survival signals. Among these signals, BAFF has a crucial role in controlling peripheral B cell homeostasis (Mackay et al., 2003). In *Rag2*^{R229Q} mice increased BAFF serum level is likely a consequence of the B cell lymphopenic environment (Lesley et al., 2004; Lavie et al., 2007). It has been shown that increased BAFF levels favor the persistence of self-reactive B cells normally deleted at developmental checkpoints (Lesley et al., 2004; Thien et al., 2004). Indeed, high levels of BAFF have been detected in the serum

of patients with various autoimmune conditions (Zhang et al., 2001; Groom et al., 2002; Lindh et al., 2008). In *Rag2*^{R229Q} mice high levels of serum BAFF might rescue autoreactive clones and favor their differentiation to ISC. We showed that blocking of BAFF-BAFF-R signaling in *Rag2*^{R229Q} mice with an anti-BAFF-R monoclonal antibody led to the disappearance of anti-dsDNA IgG antibodies, a significant amelioration of inflammatory infiltrates and an arrest of renal disease progression. Thus, these data strongly suggest that B cell abnormalities and increased BAFF serum levels play a significant role in autoimmune manifestations in *Rag2*^{R229Q} mice. Walter et al. (2010), in the companion paper, also measured elevated serum BAFF levels and autoantibody production in a large proportion of patients with OS and leaky SCID caused by hypomorphic *rag* mutations. Based on the results presented in this study, we propose that defects in B cell differentiation and function actively contribute to the OS pathogenesis. In support of this hypothesis, we reported the presence of terminally differentiated plasma cells in the lymphoid organs of OS patients devoid of circulating B cells. The similarities between murine and human studies validate the *Rag2*^{R229Q} model for further investigation on the contribution of B cell defects to autoimmunity. In conclusion, we have shown that hypomorphic *rag* mutations do not only result in profound impairment of B cell development but are also associated with the generation of an autoimmune BCR repertoire. We showed that the peripheral cytokines milieu crucially influences the generation of ISC and B cell–mediated immunopathology. The contribution of B cells to autoimmune pathology could provide the basis for a potential use of B cell–directed intervention in OS treatment.

MATERIALS AND METHODS

Patients and cells. Six unrelated patients with hypomorphic *RAG* defects whose clinical, immunological, and molecular features were consistent with OS were studied (Table S1). Human samples were collected after signed informed consent in accordance with the protocols of Spedali Civili of Brescia and Erasmus MC Ethical Committees. Mononuclear cells from peripheral blood and BM were purified on Ficoll gradient (Nycomed Pharma A/S).

Mice treatment and immunization. 129Sv/C57BL/6 knock-in *Rag2*^{R229Q} mice were previously generated (Marrella et al., 2007), and housed in specific pathogen–free facilities. Immunizations were performed in mice aged 2–3 mo. T cell–dependent antigen response was induced by footpad injection of 100 µl of a 1:1 emulsion of CFA and 100 µg OVA (grade V; Sigma-Aldrich). Secondary response was elicited by boosting with 50 µg OVA in IFA (Sigma-Aldrich). T cell–independent antigen response was induced by i.p. injection of 115 µg Pneumovax-23 (Merck). For CD4$^+$ T cell depletion, mice were injected i.v. with two doses of GK1.5 (0.25 mg) 3 wk apart and followed for a total of 7 wk. Anti–BAFF-R (9B9) mAb treatment was performed in mice (3–5 mo age) previously tested for serum autoantibody and urine proteinuria. 3 doses of 0.5 mg were administered i.v. at 3 wk intervals. The mice were followed for 2 mo. In all experiments control mice were injected with PBS. All procedures were performed according to protocols approved by the Institutional Animal Care and Use Committee of the San Raffaele Scientific Institute (IACUC318).

Proteinuria evaluation. Proteinuria was evaluated using Albustix stick (Bayer). Proteinuria index was scored as follows: 0 < 30 mg/dl; 1 = 30 mg/dl; 2 = 100 mg/dl; 3 = 300 mg/dl; and 4 ≥ 2,000 mg/dl.

Flow cytometry and cell sorting. Mononuclear cells from the peripheral blood and BM of patients were labeled with the following antibodies: anti–human-CD19, CD24, CD38, CD22 (BD); SmIgM, SmIgD, CyIgM (Kallestad/Sanofi-Synthelabo). Cell suspensions from murine BM, spleens, and LNs were stained in PBS 2% FCS-containing antibodies. To reduce nonspecific binding, cells were pretreated with anti-CD16 (BD). The following anti–mouse antibodies were purchased from eBioscience: B220, CD5, CD21, CD23, BP-1, CD40L, and PD-1. Reagents purchased from BD include: IgM, IgD, MHCII, CD40, ICOS, CD69, CD80, CD86, AA4.1, Mac-1, CD4 (RM4-5 and GK1.5), CD138, λ chain, HSA, streptavidin, and appropriate isotype controls. Anti–mouse-CD43 and CXCR5 were obtained from BioLegend. To detect cytokines production by T cells, splenocytes were cultured for 5 h with PMA (50 ng/ml), ionomycin (1 µg/ml), and monensin (1 µg/ml; Sigma Aldrich), and then intracellular IFN-γ, IL-4, IL-10, and IL-17 were stained according to the manufacturer's instructions (BD). Samples were acquired on a FACSCanto II system (BD) and analyzed with FLOWJO software (version 4.5.4; Tree Star Inc.). Splenic B lymphocytes (B220$^+$) used for mRNA analyses were sorted with a FACSAria (BD). The purity was >95%.

ELISA and ELISpot. Levels of IgG isotypes, IgA, and IgM were measured in culture supernatants and sera by multiplex assay kit (Beadlyte Mouse Immunoglobulin Isotyping kit; Millipore) according to the manufacturer's instructions and run using a Bio-Plex reader (BioRad Laboratories). Levels of IgE were determined by ELISA assay (BD). Cytokine and chemokine levels in supernatants and sera were measured with specific ELISA kits for mouse BAFF, IL-21, IFN-γ, and CXCL10 (R&D Systems). ISCs were analyzed by ELISpot using the species-specific purified and biotinylated anti-IgG, IgM, IgA, and IgE mAbs (Southern Biotech) and the 3-amino-9-ethylcarbazole (Sigma-Aldrich) as a chromogenic substrate.

Determination of auto-antibody profile. For anti-dsDNA, 1:10 diluted serum was applied to fixed *C. luciliae* slides (Antibodies Inc.), with biotin-conjugated goat anti–mouse IgG (Southern Biotech), and Alexa Fluor 555–conjugated streptavidin (Invitrogen) as detection reagent. A reader blinder to the genotype/treatment of the mice read slides at 1,000×. Anti-dsDNA antibodies were also evaluated by ELISA assay. In brief, polystyrene plates were coated with poly-L-lysine (Sigma-Aldrich) and DNA from calf thymus (Sigma-Aldrich); after post coating with 50 µg/ml of Polyglutamic Acid for 45 min and blocking with PBS 3% BSA, serial dilutions of serum from 1:20 to 1:1,280 were incubated overnight. Bound Abs were detected with alkaline phosphatase-conjugated goat anti–mouse IgG (Southern Biotech). The score of positivity was assigned to sera that were positive for dilution of 1:20 or higher. For anti-cardiolipin antibodies, polystyrene plates were coated with 50 µg/ml of cardiolipin diluted in ethyl alcohol.

Autoantibodies against murine tissues were detected by indirect immunohistochemistry on cryostat tissue sections from adult *Rag2/Il2rc*$^{-/-}$ mice to avoid interference from endogenous Ig, and stained with 1/20 dilutions of sera from *Rag2*^{R229Q} mice and control littermates. Slides were examined on a Zeiss Axioplan-2 microscope and images were acquired by Olympus DP70 camera using Cell^F imaging software (Soft Imaging System GmbH).

Functional in vitro assay. Total splenocytes were labeled with 0.5 µM CFSE (Invitrogen) for 8 min at room temperature. After quenching the labeling reaction by adding FCS, cells were washed twice. Labeled cells (10^5 cells) were cultured in a 96-well U-bottomed plate with the following stimuli: 2.5 µg/ml CpG-B oligodeoxynucleotide (5′-tccatgacgttcctgacgtt-3′; Alexis Co.), 10 µg/ml LPS (R&D Systems), and 10 ng/ml IL-4 (R&D Systems). The proliferation profile of propidium iodide-negative viable B220$^+$ cells was analyzed at day 4 of culture. On the same day, culture supernatants were collected for Ig quantification.

Histology. Formalin-fixed paraffin-embedded tissue sections from inguinal LN biopsies of OS patients and patients with unrelated nonimmunological diseases were subjected to routine hematoxylin and eosin (H&E) and double

immunostains. In brief, sections were de-waxed, rehydrated, and endogenous peroxidase activity blocked before heat-induced epitope retrieval in 1.0 mM EDTA buffer (pH 8.0) followed by 1 h incubation with primary monoclonal mouse anti–human CD138 (clone NI15, 1:100; Dako) and rat monoclonal anti–Blimp-1 (clone 6D3, 1:50; Santa Cruz Biotechnology Inc.) antibodies. Double immunostainings were obtained by combining a first step using the appropriate biotinylated secondary anti–rat antibody (1:100; Vector Laboratories) followed by streptavidin (SA)-conjugated HRP and diaminobenzidine (Dako) as chromogen, and a second step using a biotinylated secondary anti–mouse antibody (1:100; Vector Laboratories) followed by SA-conjugated alkaline phosphatase (Dako) and Ferangi Blue as chromogen (Biocare Medical). Nuclei were counterstained with Methyl Green.

Formalin fixed paraffin embedded murine samples (liver, kidney, skin, lung, and gut) were subjected to H&E staining to check for basic histopathological changes, and immunohistochemistry was performed as previously described for human samples. Single immunostain reactivity was revealed using Real EnVision Mouse/Rabbit-HRP (Dako) or Super Sensitive IHC Detection System (BioGenex), followed by diaminobenzidine and nuclei counterstained with H&E. The following primary antibodies have been used: monoclonal rat anti-CD3ε (clone CT-CD3; 1:100; Valter Occhiena), rat anti-B220 (clone RA3-6B2; 1:100; Valter Occhiena), rat anti-F4/80 (clone BM8; 1:25; Caltag Laboratories), and polyclonal rabbit anti-Iba-1 (1:400; Wako). Murine plasma cells and Ig deposits have been detected directly by using either an appropriate biotinylated secondary goat anti-murine IgM (Dako) and goat anti–murine IgG (H+L; KPL) or ChemMATE Envision Mouse-HRP detection system (Dako) that bind specifically to the murine Ig. Digital images were then acquired with Olympus DP70 camera mounted on Olympus Bx60 microscope using AnalySIS imaging software (Soft Imaging System GmbH).

The degree of inflammation in the liver, lung, and kidney was double-blinded scored using the following criteria: 0 (none or scarse cell infiltrates); 1 (low to moderate); 2 (moderate to high); 3 (very high). Colitis was graded as follows (Scheiffele and Fuss, 2002): grade 0, no evidence of inflammation; grade 1, low level of leukocyte infiltration around the crypt basis in <10% HPF with no structural changes; grade 2, moderate infiltration in 10–25% HPF involving the lamina propria with minimal epithelial hyperplasia and/or goblet cell depletion; grade 3, high level of infiltration in 25–50% HPF reaching the muscularis mucosa with bowel wall thickening, moderate goblet cell loss, edema, crypt elongation, and epithelial erosions; grade 4: marked degree of transmural infiltration in >50% HPF with massive loss of goblet cell, fibrosis, elongated and distorted crypts with occasional abscesses, ulcerations, and bowel-wall thickening.

Ig genes amplification. For bulk *Igh* PCRs splenic B220$^+$ cells from WT and *Rag2*^{R229Q} mice were sorted on a FACS Aria (BD), excluding cell doublets, into 96-well PCR plates (Applied Biosystems; 50 cells/well) containing 20 µl/well of ice-cold 0.5× PBS supplemented with 10 mM DTT, 8 U RNAsin (Promega), and 0.4 U 5′-Prime RNase Inhibitor (Eppendorf). Plates were sealed and immediately frozen on dry ice before storage at −80°C. cDNA was synthesized in a total volume of 40 µl/well in the original 96-well sorting plate. The reverse transcription (RT) reaction was performed by using the High Capacity cDNA Archive kit (Applied Biosystems) following manufacturer's instructions. cDNA was stored at −20°C. *Igh* transcripts were amplified by PCR using 3 µl of cDNA as template. All reactions were performed in PCR tubes in a total volume of 50 µl per well containing 100 nM of each primer (msVHE and mCh-mu-inner), 200 µM each dNTP (Invitrogen), and 1.25U HotStar Taq DNA polymerase (QIAGEN). Primers were stored in small aliquots to avoid repeated freezing and thawing and all PCRs were performed with nuclease-free water. PCR was performed for 35 cycles at 95°C for 30 s, 56°C for 30 s, and 72°C for 55 s. For single-cell *Igh* PCRs the experimental procedures have been described in detail before (Tiller et al., 2009). In brief, single B220$^+$CD19$^+$ splenocytes were sorted on FACSV antage with DiVa option (BD), using doublet discrimination and single-cell sorting mask settings. Cells were sorted into 96-well plates (Eppendorf) containing 4 µl of 0.5× PBS supplemented with 10 mM DTT (Invitrogen) and 8 U RNAsin (Promega). Synthesis of cDNA was performed in the 96-well plates used for sorting in a total volume of 15 µl containing random hexamer primers (5 µM; Roche), NP-40 (0.3% vol/vol; Sigma-Aldrich), 10 mM DTT, 36 U RNAsin, dNTPs (833 µM of each nucleotide; Invitrogen), and 50 U SuperScript III reverse transcription (Invitrogen). Reverse transcription was performed at 42°C for 5 min, 25°C for 10 min, 50°C for 60 min, and 94°C for 5 min. A semi-nested PCR strategy was used for amplification of *Igh* transcripts from single cells. First round PCR was performed in a total volume of 40 µl, containing 3.5 µl product of the RT reaction, msVHE and mCh-mu-outer primers (150 nM each), dNTPs (250 µM of each nucleotide), and 1 U HotStar Taq Polymerase. The reaction was performed for 50 cycles at 94°C for 30 s, 56°C for 30 s, and 72°C for 55 s. Second round PCR was performed in a total volume of 40 µl, containing 3.5 µl product of the first round reaction, msVHE and mCh-mu-inner primers (150 nM each), dNTPs (250 µM of each nucleotide), and 1 U HotStar Taq Polymerase. The reaction was performed for 50 cycles at 94°C for 30 s, 60°C for 30 s, and 72°C for 45 s.

The primers used are as follows: msVHE, 5′-GGGAATTCGAGGTGCAGCTGCAGGAGTCTGG-3′; mCh-mu-outer, 5′-AGGGGGCTCTCGCAGGAGACGAGG-3′; mCh-mu-inner, 5′-AGGGGGAAGACATTTGGGAAGGAC-3′.

PCR products were then cloned into a pCR2.1-TOPO TA vector. Ligation was performed in a total volume of 10 µl with 1U T4-Ligate (Invitrogen), 2 µl PCR product, and 50 ng linearized vector. Competent *E. coli* TOP10F' bacteria (Takara Bio Inc.) were transformed at 42°C with 10 µl of the ligation product. Colonies were screened by blue–white selection. Sequencing of plasmids and PCR products was performed using vector primer and msVHE, respectively. For analysis of bulk populations, identical nucleotide sequences generated from the same PCR well were excluded from the analysis. The obtained sequences were analyzed using National Center for Biotechnology Information IgBLAST (http://ncbi.nlm.nih.gov/projects/igblast/). Sequences were assigned to the *Igh*-V segment yielding the highest score, in case of a tie between several segments, the segment using the canonical nomenclature (<*Igh*-V segment family>.<segment number within family>.<segment number within locus>; Johnston et al., 2006) was assigned. Because of the genetic background of the animals (BX129 or 129XB), no discrimination between segments of the *Igh*^{a} (129) and *Igh*^{b} (B6) allele were made. *Igh*-D segments were only assigned if they showed at least six matching bases. Mismatches of the obtained sequences versus the known germline sequence were counted as hypermutations.

RNA extraction and real-time PCR. Total RNA from sorted B220$^+$ cells of pooled mice (n = 5/group) was extracted using a conventional TRIzol-extraction (Invitrogen), treated with 100 U/ml Dnase I (Invitrogen), and reverse transcribed using the High Capacity cDNA Archive kit (Applied Biosystems). Expression of *Prmd1/Blimp1* (Mm00476128_m1), *Xbp1* (Mm 00457359_m1), *Aicda* (Mm00507774_m1), *Tlr4* (Mm00445274_m1), and *Tlr9* (Mm 00446193_m1) was quantified using the Assay on Demand kit (Applied Biosystems) and TaqMan Universal PCR mastermix (Applied Biosystems). qPCR was performed by using an ABI 7900 and analyzed using SDS version 2.3 (Applied Biosystems). cMyc, Bcl-6, T-bet, RORγT, Gata-3, and Cxcl2 expression was quantified by RT-qPCR from 50 ng cDNA in the presence of the TaqMan Universal PCR mastermix, 200 nM gene-specific TaqMan probe (Universal Probes; Roche), and 800 nM of relative primer pairs, using the DNA Engine Opticon 2 System (MJ Research). Thermal cycle conditions were the following: 95°C for 10 min, 40 cycles of 95°C for 15 s, and 60°C for 60 s. The primers and probes used are as follows: *c-Myc*, 5′-CCTAGTGCTGCATGAGGAGA-3′ and 5′-TCTTCCTCATCTTCTTGCTCTTC-3′, probe #77; *Bcl6*, 5′-TTCCGCTACAAGGGCAAC-3′ and 5′-CAGCGATAGGGTTTCTCACC-3′, probe #5 ; *T-bet*, 5′-TCAACCAGCACCAGACAGAG-3′ and 5′-AAACATCCTGTAATGGCTTGTG-3′, probe #19; *RORγT*, 5′-CGACTGGAGGACCTTCTACG-3′ and 5′-CCCACATCTCCCACATTGA-3′, probe #52; *Gata-3*, 5′-TTATCAAGCCCAAGCGAAG-3′ and 5′-TGGTGGTGGTCTGACAGTTC-3′, probe #108; *Cxc12*, 5′-CTGTGCCCTTCAGATTGTTG-3′ and 5′-TAATTTCGGGTCAATGCACA-3′, probe #41;

Cyclophilin, 5′-TTCAAGCTGAAGCACTACGG-3′ and 5′-ATTGGTGTCTTTGCCTGCAT-3′, probe #20. Each sample was analyzed in duplicates, and the relative expression of target genes were defined by calculating the Δcycle threshold, with respect to the housekeeping gene.

Statistical analysis. Data were compared by a two-tailed Mann-Whitney *U* test. P values of <0.05 were considered significant. P values for Ig gene repertoire analyses were calculated by 2 × 2 Fisher's exact test.

Online supplemental material. Fig. S1 shows the frequencies and absolute counts of different B cell subsets in BM and spleen. Fig. S2 shows the analysis of the *Igh* repertoire and clonal relationships of splenic B cells of mutant and WT animals. Fig. S3A illustrates that a higher proportion of ISC is present in the lymphoid tissues of *Rag2*^{R229Q} mice. Fig. S3B shows defective CXCL12 expression in the BM of *Rag2*^{R229Q} mice. Fig. S4 shows the expression of costimulatory molecules by CXCR5^{+} ICOS^{+} CD4^{+} T_{FH} cells. Fig. S5 describes the short-term humoral response to TI antigen. Fig. S6A shows that high serum concentration of the chemokine CXCL10 is present in *Rag2*^{R229Q} mice. Fig. S6B shows B cell infiltrates in the liver of mutant mice. Fig. S6C illustrates the degree of cell-specific infiltrates in different organs of mutant mice. Fig. S6D demonstrates that high BAFF serum level is already present in young *Rag2*^{R229Q} mice. Table S1 shows the clinical and genetic features of OS patients included in the study. Table S2 indicates that *Rag2*^{R229Q} mice have a restricted B cell repertoire. Online supplemental material is available at http://www.jem.org/cgi/content/full/jem.20091928/DC1.

The technical assistance of Massimiliano Mirolo, Lucia Susani, and Enrica Mira Catò is acknowledged.

This work was supported by grants from the Fondazione Telethon to A. Villa and from the Fondazione Cariplo to A. Villa, P.L. Poliani, and F. Grassi. FIRB grant RBIN04CHXT to P. Vezzoni and ERA/NET "Autoimmune liver disease" to A. Villa partially contributed to the study.

The authors have no financial conflicts of interest.

Submitted: 3 September 2009
Accepted: 14 May 2010

REFERENCES

Agenès, F., and A.A. Freitas. 1999. Transfer of small resting B cells into immunodeficient hosts results in the selection of a self-renewing activated B cell population. *J. Exp. Med.* 189:319–330. doi:10.1084/jem.189.2.319

Angelin-Duclos, C., G. Cattoretti, K.I. Lin, and K. Calame. 2000. Commitment of B lymphocytes to a plasma cell fate is associated with Blimp-1 expression in vivo. *J. Immunol.* 165:5462–5471.

Bauquet, A.T., H. Jin, A.M. Paterson, M. Mitsdoerffer, I.C. Ho, A.H. Sharpe, and V.K. Kuchroo. 2009. The costimulatory molecule ICOS regulates the expression of c-Maf and IL-21 in the development of follicular T helper cells and TH-17 cells. *Nat. Immunol.* 10:167–175. doi:10.1038/ni.1690

Cassani, B., P.L. Poliani, D. Moratto, C. Sobacchi, V. Marrella, L. Imperatori, D. Vairo, A. Plebani, S. Giliani, P. Vezzoni, et al. 2010. Defect of regulatory T cells in patients with Omenn syndrome. *J. Allergy Clin. Immunol.* 125:209–216. doi:10.1016/j.jaci.2009.10.023

Chtanova, T., S.G. Tangye, R. Newton, N. Frank, M.R. Hodge, M.S. Rolph, and C.R. Mackay. 2004. T follicular helper cells express a distinctive transcriptional profile, reflecting their role as non-Th1/Th2 effector cells that provide help for B cells. *J. Immunol.* 173:68–78.

Groom, J., S.L. Kalled, A.H. Cutler, C. Olson, S.A. Woodcock, P. Schneider, J. Tschopp, T.G. Cachero, M. Batten, J. Wheway, et al. 2002. Association of BAFF/BLyS overexpression and altered B cell differentiation with Sjögren's syndrome. *J. Clin. Invest.* 109:59–68.

Hardy, R.R., C.E. Carmack, S.A. Shinton, J.D. Kemp, and K. Hayakawa. 1991. Resolution and characterization of pro–B and pre–pro–B cell stages in normal mouse bone marrow. *J. Exp. Med.* 173:1213–1225. doi:10.1084/jem.173.5.1213

Harfst, E., J. Andersson, U. Grawunder, R. Ceredig, and A.G. Rolink. 2005. Homeostatic and functional analysis of mature B cells in lambda5-deficient mice. *Immunol. Lett.* 101:173–184. doi:10.1016/j.imlet.2005.05.013

Harville, T.O., D.M. Adams, T.A. Howard, and R.E. Ware. 1997. Oligoclonal expansion of CD45RO+ T lymphocytes in Omenn syndrome. *J. Clin. Immunol.* 17:322–332. doi:10.1023/A:1027330800085

Hillion, S., C. Rochas, P. Youinou, and C. Jamin. 2005. Expression and reexpression of recombination activating genes: relevance to the development of autoimmune states. *Ann. N. Y. Acad. Sci.* 1050:10–18. doi:10.1196/annals.1313.002

Hutloff, A., K. Büchner, K. Reiter, H.J. Baelde, M. Odendahl, A. Jacobi, T. Dörner, and R.A. Kroczek. 2004. Involvement of inducible costimulator in the exaggerated memory B cell and plasma cell generation in systemic lupus erythematosus. *Arthritis Rheum.* 50:3211–3220. doi:10.1002/art.20519

Iwai, H., M. Abe, S. Hirose, F. Tsushima, K. Tezuka, H. Akiba, H. Yagita, K. Okumura, H. Kohsaka, N. Miyasaka, and M. Azuma. 2003. Involvement of inducible costimulator-B7 homologous protein costimulatory pathway in murine lupus nephritis. *J. Immunol.* 171:2848–2854.

Johnston, C.M., A.L. Wood, D.J. Bolland, and A.E. Corcoran. 2006. Complete sequence assembly and characterization of the C57BL/6 mouse Ig heavy chain V region. *J. Immunol.* 176:4221–4234.

Keenan, R.A., A. De Riva, B. Corleis, L. Hepburn, S. Licence, T.H. Winkler, and I.L. Mårtensson. 2008. Censoring of autoreactive B cell development by the pre-B cell receptor. *Science.* 321:696–699. doi:10.1126/science.1157533

Khiong, K., M. Murakami, C. Kitabayashi, N. Ueda, S. Sawa, A. Sakamoto, B.L. Kotzin, S.J. Rozzo, K. Ishihara, M. Verella-Garcia, et al. 2007. Homeostatically proliferating CD4 T cells are involved in the pathogenesis of an Omenn syndrome murine model. *J. Clin. Invest.* 117:1270–1281. doi:10.1172/JCI30513

Kobayashi, S., N. Haruo, K. Sugane, H.D. Ochs, and K. Agematsu. 2009. Interleukin-21 stimulates B-cell immunoglobulin E synthesis in human beings concomitantly with activation-induced cytidine deaminase expression and differentiation into plasma cells. *Hum. Immunol.* 70:35–40. doi:10.1016/j.humimm.2008.10.021

Korn, T., E. Bettelli, W. Gao, A. Awasthi, A. Jäger, T.B. Strom, M. Oukka, and V.K. Kuchroo. 2007. IL-21 initiates an alternative pathway to induce proinflammatory T(H)17 cells. *Nature.* 448:484–487. doi:10.1038/nature05970

Krieg, A.M., A.K. Yi, S. Matson, T.J. Waldschmidt, G.A. Bishop, R. Teasdale, G.A. Koretzky, and D.M. Klinman. 1995. CpG motifs in bacterial DNA trigger direct B-cell activation. *Nature.* 374:546–549. doi:10.1038/374546a0

Lavie, F., C. Miceli-Richard, M. Ittah, J. Sellam, J.E. Gottenberg, and X. Mariette. 2007. Increase of B cell-activating factor of the TNF family (BAFF) after rituximab treatment: insights into a new regulating system of BAFF production. *Ann. Rheum. Dis.* 66:700–703. doi:10.1136/ard.2006.060772

Lesley, R., Y. Xu, S.L. Kalled, D.M. Hess, S.R. Schwab, H.B. Shu, and J.G. Cyster. 2004. Reduced competitiveness of autoantigen-engaged B cells due to increased dependence on BAFF. *Immunity.* 20:441–453. doi:10.1016/S1074-7613(04)00079-2

Lin, Y., Wong, K., and Calame, K. 1997. Repression of c-myc transcription by Blimp-1, an inducer of terminal B cell differentiation. *Science.* 276:596-599. doi:10.1126/science.276.5312.596

Lindh, E., S.M. Lind, E. Lindmark, S. Hässler, J. Perheentupa, L. Peltonen, O. Winqvist, and M.C. Karlsson. 2008. AIRE regulates T-cell-independent B-cell responses through BAFF. *Proc. Natl. Acad. Sci. USA.* 105:18466–18471. doi:10.1073/pnas.0808205105

Mackay, F., and H. Leung. 2006. The role of the BAFF/APRIL system on T cell function. *Semin. Immunol.* 18:284–289. doi:10.1016/j.smim.2006.04.005

Mackay, F., P. Schneider, P. Rennert, and J. Browning. 2003. BAFF AND APRIL: a tutorial on B cell survival. *Annu. Rev. Immunol.* 21:231–264. doi:10.1146/annurev.immunol.21.120601.141152

Mackay, F., S.A. Woodcock, P. Lawton, C. Ambrose, M. Baetscher, P. Schneider, J. Tschopp, and J.L. Browning. 1999. Mice transgenic for BAFF develop lymphocytic disorders along with autoimmune manifestations. *J. Exp. Med.* 190:1697–1710. doi:10.1084/jem.190.11.1697

Mak, T.W., A. Shahinian, S.K. Yoshinaga, A. Wakeham, L.M. Boucher, M. Pintilie, G. Duncan, B.U. Gajewska, M. Gronski, U. Eriksson, et al. 2003. Costimulation through the inducible costimulator ligand is essential for both T helper and B cell functions in T cell-dependent B cell responses. *Nat. Immunol.* 4:765–772. doi:10.1038/ni947

Manson, J.J., A. Ma, P. Rogers, L.J. Mason, J.H. Berden, J. van der Vlag, D.P. D'Cruz, D.A. Isenberg, and A. Rahman. 2009. Relationship between anti-dsDNA, anti-nucleosome and anti-alpha-actinin antibodies and markers of renal disease in patients with lupus nephritis: a prospective longitudinal study. *Arthritis Res. Ther.* 11:R154. doi:10.1186/ar2831

Marrella, V., P.L. Poliani, A. Casati, F. Rucci, L. Frascoli, M.L. Gougeon, B. Lemercier, M. Bosticardo, M. Ravanini, M. Battaglia, et al. 2007. A hypomorphic R229Q Rag2 mouse mutant recapitulates human Omenn syndrome. *J. Clin. Invest.* 117:1260–1269. doi:10.1172/JCI30928

Martins, G., and K. Calame. 2008. Regulation and functions of Blimp-1 in T and B lymphocytes. *Annu. Rev. Immunol.* 26:133–169. doi:10.1146/annurev.immunol.26.021607.090241

Meyer-Bahlburg, A., S.F. Andrews, K.O. Yu, S.A. Porcelli, and D.J. Rawlings. 2008. Characterization of a late transitional B cell population highly sensitive to BAFF-mediated homeostatic proliferation. *J. Exp. Med.* 205:155–168. doi:10.1084/jem.20071088

Münz, C., J.D. Lünemann, M.T. Getts, and S.D. Miller. 2009. Antiviral immune responses: triggers of or triggered by autoimmunity? *Nat. Rev. Immunol.* 9:246–258. doi:10.1038/nri2527

Noordzij, J.G., S. de Bruin-Versteeg, N.S. Verkaik, J.M. Vossen, R. de Groot, E. Bernatowska, A.W. Langerak, D.C. van Gent, and J.J. van Dongen. 2002. The immunophenotypic and immunogenotypic B-cell differentiation arrest in bone marrow of RAG-deficient SCID patients corresponds to residual recombination activities of mutated RAG proteins. *Blood.* 100:2145–2152.

Nurieva, R.I., Y. Chung, G.J. Martinez, X.O. Yang, S. Tanaka, T.D. Matskevitch, Y.H. Wang, and C. Dong. 2009. Bcl6 mediates the development of T follicular helper cells. *Science.* 325:1001–1005. doi:10.1126/science.1176676

Ochs, H.D., S.D. Davis, E. Mickelson, K.G. Lerner, and R.J. Wedgwood. 1974. Combined immunodeficiency and reticuloendotheliosis with eosinophilia. *J. Pediatr.* 85:463–465. doi:10.1016/S0022-3476(74)80445-2

Omenn, G.S. 1965. Familial Reticuloendotheliosis with Eosinophilia. *N. Engl. J. Med.* 273:427–432.

Pasare, C., and R. Medzhitov. 2005. Control of B-cell responses by Toll-like receptors. *Nature.* 438:364–368. doi:10.1038/nature04267

Poliani, P.L., F. Facchetti, M. Ravanini, A.R. Gennery, A. Villa, C.M. Roifman, and L.D. Notarangelo. 2009. Early defects in human T-cell development severely affect distribution and maturation of thymic stromal cells: possible implications for the pathophysiology of Omenn syndrome. *Blood.* 114:105–108. doi:10.1182/blood-2009-03-211029

Rauch, M., R. Tussiwand, N. Bosco, and A.G. Rolink. 2009. Crucial role for BAFF-BAFF-R signaling in the survival and maintenance of mature B cells. *PLoS One.* 4:e5456. doi:10.1371/journal.pone.0005456

Reimold, A.M., N.N. Iwakoshi, J. Manis, P. Vallabhajosyula, E. Szomolanyi-Tsuda, E.M. Gravallese, D. Friend, M.J. Grusby, F. Alt, and L.H. Glimcher. 2001. Plasma cell differentiation requires the transcription factor XBP-1. *Nature.* 412:300–307. doi:10.1038/35085509

Rieux-Laucat, F., P. Bahadoran, N. Brousse, F. Selz, A. Fischer, F. Le Deist, and J.P. De Villartay. 1998. Highly restricted human T cell repertoire in peripheral blood and tissue-infiltrating lymphocytes in Omenn's syndrome. *J. Clin. Invest.* 102:312–321. doi:10.1172/JCI332

Schaerli, P., K. Willimann, A.B. Lang, M. Lipp, P. Loetscher, and B. Moser. 2000. CXC chemokine receptor 5 expression defines follicular homing T cells with B cell helper function. *J. Exp. Med.* 192:1553–1562. doi:10.1084/jem.192.11.1553

Scheiffele, F., and I.J. Fuss. 2002. Induction of TNBS colitis in mice. *Curr. Protocol. Immunol.* 15:15.

Shaffer, A.L., K.I. Lin, T.C. Kuo, X. Yu, E.M. Hurt, A. Rosenwald, J.M. Giltnane, L. Yang, H. Zhao, K. Calame, and L.M. Staudt. 2002. Blimp-1 orchestrates plasma cell differentiation by extinguishing the mature B cell gene expression program. *Immunity.* 17:51–62. doi:10.1016/S1074-7613(02)00335-7

Shaffer, A.L., M. Shapiro-Shelef, N.N. Iwakoshi, A.H. Lee, S.B. Qian, H. Zhao, X. Yu, L. Yang, B.K. Tan, A. Rosenwald, et al. 2004. XBP1, downstream of Blimp-1, expands the secretory apparatus and other organelles, and increases protein synthesis in plasma cell differentiation. *Immunity.* 21:81–93. doi:10.1016/j.immuni.2004.06.010

Shaffer, A.L., X. Yu, Y. He, J. Boldrick, E.P. Chan, and L.M. Staudt. 2000. BCL-6 represses genes that function in lymphocyte differentiation, inflammation, and cell cycle control. *Immunity.* 13:199–212. doi:10.1016/S1074-7613(00)00020-0

Signorini, S., L. Imberti, S. Pirovano, A. Villa, F. Facchetti, M. Ungari, F. Bozzi, A. Albertini, A.G. Ugazio, P. Vezzoni, and L.D. Notarangelo. 1999. Intrathymic restriction and peripheral expansion of the T-cell repertoire in Omenn syndrome. *Blood.* 94:3468–3478.

Sobacchi, C., V. Marrella, F. Rucci, P. Vezzoni, and A. Villa. 2006. RAG-dependent primary immunodeficiencies. *Hum. Mutat.* 27:1174–1184. doi:10.1002/humu.20408

Sobel, E.S., T. Katagiri, K. Katagiri, S.C. Morris, P.L. Cohen, and R.A. Eisenberg. 1991. An intrinsic B cell defect is required for the production of autoantibodies in the lpr model of murine systemic autoimmunity. *J. Exp. Med.* 173:1441–1449. doi:10.1084/jem.173.6.1441

Szabo, S.J., B.M. Sullivan, C. Stemmann, A.R. Satoskar, B.P. Sleckman, and L.H. Glimcher. 2002. Distinct effects of T-bet in TH1 lineage commitment and IFN-gamma production in CD4 and CD8 T cells. *Science.* 295:338–342. doi:10.1126/science.1065543

Thien, M., T.G. Phan, S. Gardam, M. Amesbury, A. Basten, F. Mackay, and R. Brink. 2004. Excess BAFF rescues self-reactive B cells from peripheral deletion and allows them to enter forbidden follicular and marginal zone niches. *Immunity.* 20:785–798. doi:10.1016/j.immuni.2004.05.010

Tiller, T., C.E. Busse, and H. Wardemann. 2009. Cloning and expression of murine Ig genes from single B cells. *J. Immunol. Methods.* 350:183–193. doi:10.1016/j.jim.2009.08.009

Tokoyoda, K., T. Egawa, T. Sugiyama, B.I. Choi, and T. Nagasawa. 2004. Cellular niches controlling B lymphocyte behavior within bone marrow during development. *Immunity.* 20:707–718. doi:10.1016/j.immuni.2004.05.001

Ueda, Y., D. Liao, K. Yang, A. Patel, and G. Kelsoe. 2007. T-independent activation-induced cytidine deaminase expression, class-switch recombination, and antibody production by immature/transitional 1 B cells. *J. Immunol.* 178:3593–3601.

van Zelm, M.C., M. van der Burg, D. de Ridder, B.H. Barendregt, E.F. de Haas, M.J. Reinders, A.C. Lankester, T. Révész, F.J. Staal, and J.J. van Dongen. 2005. Ig gene rearrangement steps are initiated in early human precursor B cell subsets and correlate with specific transcription factor expression. *J. Immunol.* 175:5912–5922.

Vela, J.L., D. Aït-Azzouzene, B.H. Duong, T. Ota, and D. Nemazee. 2008. Rearrangement of mouse immunoglobulin kappa deleting element recombining sequence promotes immune tolerance and lambda B cell production. *Immunity.* 28:161–170. doi:10.1016/j.immuni.2007.12.011

Villa, A., L.D. Notarangelo, and C.M. Roifman. 2008. Omenn syndrome: inflammation in leaky severe combined immunodeficiency. *J. Allergy Clin. Immunol.* 122:1082–1086. doi:10.1016/j.jaci.2008.09.037

Villa, A., S. Santagata, F. Bozzi, S. Giliani, A. Frattini, L. Imberti, L.B. Gatta, H.D. Ochs, K. Schwarz, L.D. Notarangelo, et al. 1998. Partial V(D)J recombination activity leads to Omenn syndrome. *Cell.* 93:885–896. doi:10.1016/S0092-8674(00)81448-8

Villa, A., S. Santagata, F. Bozzi, L. Imberti, and L.D. Notarangelo. 1999. Omenn syndrome: a disorder of Rag1 and Rag2 genes. *J. Clin. Immunol.* 19:87–97. doi:10.1023/A:1020550432126

Villa, A., C. Sobacchi, L.D. Notarangelo, F. Bozzi, M. Abinun, T.G. Abrahamsen, P.D. Arkwright, M. Baniyash, E.G. Brooks, M.E. Conley, et al. 2001. V(D)J recombination defects in lymphocytes due to RAG mutations: severe immunodeficiency with a spectrum of clinical presentations. *Blood.* 97:81–88. doi:10.1182/blood.V97.1.81

Vinuesa, C.G., S.G. Tangye, B. Moser, and C.R. Mackay. 2005. Follicular B helper T cells in antibody responses and autoimmunity. *Nat. Rev. Immunol.* 5:853–865. doi:10.1038/nri1714

Walter, J.E., F. Rucci, L. Patrizi, M. Recher, S. Regenass, T. Paganini, M. Keszei, I. Pessach, P.A. Lang, P.L. Poliani, S. Giliani, W. Al-Herz, M.J. Cowan, J.M. Puck, J. Bleesing, T. Niehues, C. Schuetz,

Downloaded from jem.rupress.org on June 19, 2010

H. Malech, S.S. DeRavin, F. Facchetti, A.R. Gennery, E. Andersson, N.R. Kamani, J. Sekiguchi, H.M. Alenezi, J. Chinen, G. Dbaibo, G. ElGhazali, A. Fontana, S. Pasic, C. Detre, C. Terhorst, F.W. Alt, and L.D. Notarangelo. 2010. Expansion of immunoglobulin-secreting cells and defects in B cell tolerance in Rag-dependent immunodeficiency. *J. Exp. Med.* 207:■■■–■■■.

Wang, Y., G. Huang, J. Wang, H. Molina, D.D. Chaplin, and Y.X. Fu. 2000. Antigen persistence is required for somatic mutation and affinity maturation of immunoglobulin. *Eur. J. Immunol.* 30:2226–2234.

Wang, Y.H., and B. Diamond. 2008. B cell receptor revision diminishes the autoreactive B cell response after antigen activation in mice. *J. Clin. Invest.* 118:2896–2907. doi:10.1172/JCI35618

Watson, J. 1979. Continuous proliferation of murine antigen-specific helper T lymphocytes in culture. *J. Exp. Med.* 150:1510–1519. doi:10.1084/jem.150.6.1510

Zhang, J., V. Roschke, K.P. Baker, Z. Wang, G.S. Alarcón, B.J. Fessler, H. Bastian, R.P. Kimberly, and T. Zhou. 2001. Cutting edge: a role for B lymphocyte stimulator in systemic lupus erythematosus. *J. Immunol.* 166:6–10.

Zhou, L., I.I. Ivanov, R. Spolski, R. Min, K. Shenderov, T. Egawa, D.E. Levy, W.J. Leonard, and D.R. Littman. 2007. IL-6 programs T(H)-17 cell differentiation by promoting sequential engagement of the IL-21 and IL-23 pathways. *Nat. Immunol.* 8:967–974. doi:10.1038/ni1488

The Journal of Experimental Medicine

SUPPLEMENTAL MATERIAL

Cassani et al., http://www.jem.org/jem.20091928/DC1

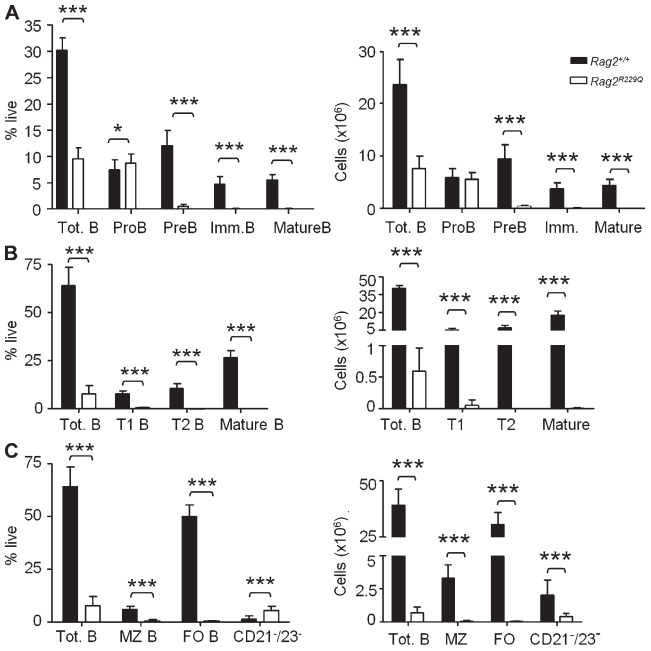

Figure S1. Characterization of B cell compartments in *Rag2*^{R229Q} mice. (A) BM B cell immunophenotype in WT mice (n = 35) and *Rag2*^{R229Q} mice (n = 42). Frequencies of different B cell subsets in BM, indicated as percentage of live cells, and absolute counts are reported. (B and C) Peripheral B cell immunophenotype in mice in WT (n = 43) and *Rag2*^{R229Q} (n = 57) mice. Mice were analyzed in six independent experiments. (B) Frequencies and absolute counts of transitional and mature B cells in the spleen using IgD and IgM markers. (C) Frequencies and absolute counts of splenic B cell populations as defined by expression of CD21 and CD23 markers within the B220$^+$ cell gate. *, $P < 0.05$; ***, $P \leq 0.001$.

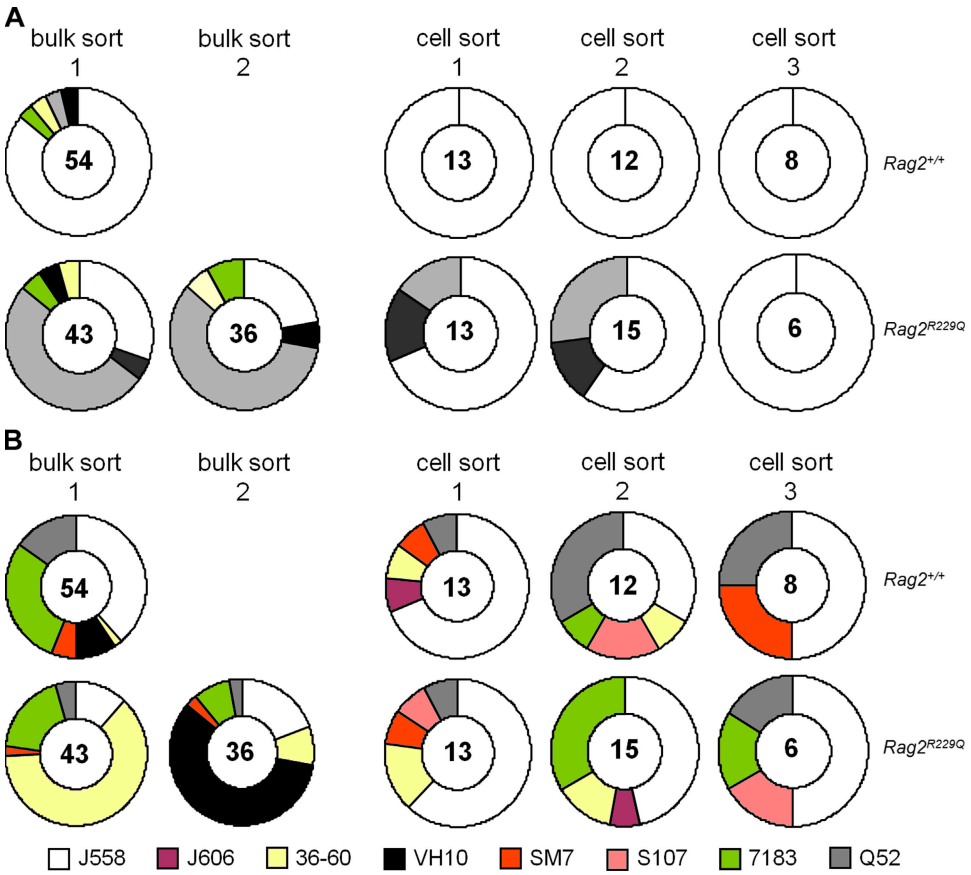

Figure S2. *Rag2*^{R229Q} mice show expansion of CRCs. Analysis of the *Igh* repertoire and clonal relationships of splenic B cells from mutant and WT animals. Transcripts encoding the IgH variable domain were amplified via RT-PCR from either bulk sorted (50 cells/well) or single-cell sorted splenic B cells. The total number of sequences analyzed from the individual animals is indicated in the center of the pie charts. (A) CRCs present in the analyzed sequences. White areas indicate unique sequences, whereas clusters of CRCs are shown in different colors. None of the CRCs depicted was shared between individual mice. (B) Usage of *Igh*-V segment families.

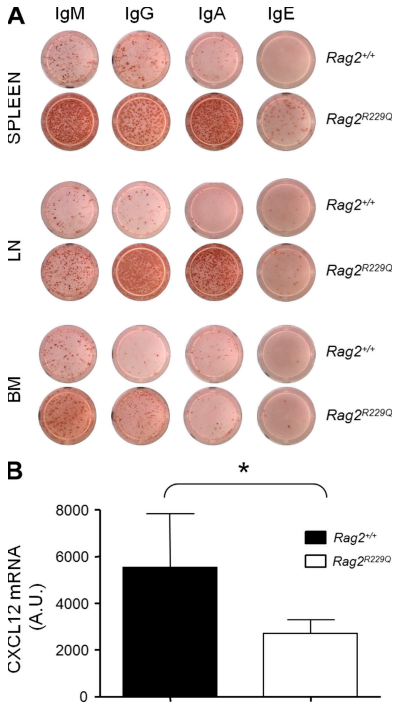

Figure S3. Higher proportion of Ig secreting cells are present in the lymphoid tissues of *Rag2*^{R229Q} mice. (A) Cell suspensions (2×10^5 cells/well) from spleen, LN, and BM of WT and *Rag2*^{R229Q} mice were cultured overnight in completed medium in the 96-well ELISpot plates. Representative images of plate wells analyzed using the ELISpot reader are shown. The data are representative of six independent experiments (3–4 mice /experiment). (B) Reduced expression of CXCL12 is present in the BM of *Rag2*^{R229Q} mice. The expression of CXCL12 was analyzed by quantitative RT-PCR in BM-derived total mononuclear cells from WT ($n = 7$) and mutant ($n = 10$) mice, and normalized to the *Ppia* mRNA. Quantitative RT-PCR was run in duplicate in three independent experiments. Results are expressed as arbitrary units (A.U.). *, $P < 0.05$.

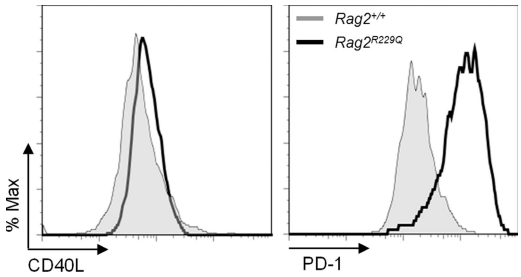

Figure S4. Phenotypic characterization of T_{FH} cells. Expression of CD40L and PD-1 markers on gated CXCR5$^+$ ICOS$^+$ CD4$^+$ T cells. Histogram plots are representative of four independent experiments.

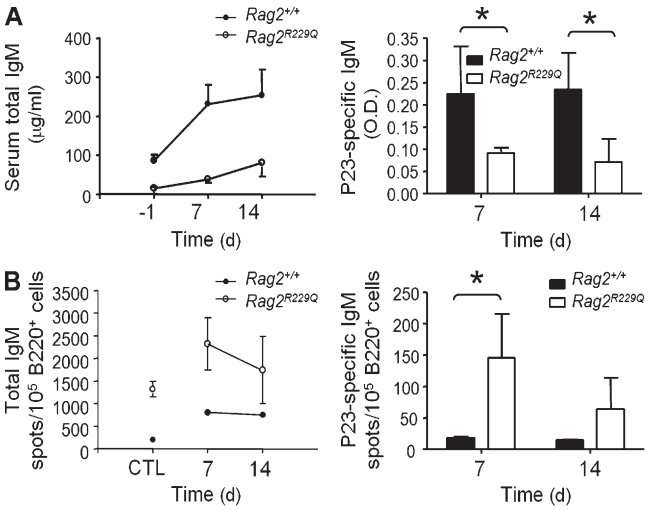

Figure S5. ***Rag2^{R229Q}* mice show enhanced humoral response to Pneumovax23.** WT and *Rag2^{R229Q}* mice were immunized i.p. with P23. PBS was injected in control mice. Total (A) and anti-P23 specific IgM (B) antibody titers were determined at days 7 and 14 after challenge by ELISA. Each group represents mean values ± SD from $n = 4$ mice and were corrected for background binding. Elispot analysis of total (C) and P23-specific (D) IgM secretion by splenocytes from WT and *Rag2^{R229Q}* mice at the indicated times after antigen challenge. Data represent the mean ± SD number of spots obtained from $n = 4$ mice/group and normalized to 10^5 B220$^+$ cells. The data are representative of two independent experiments. *, $P < 0.05$.

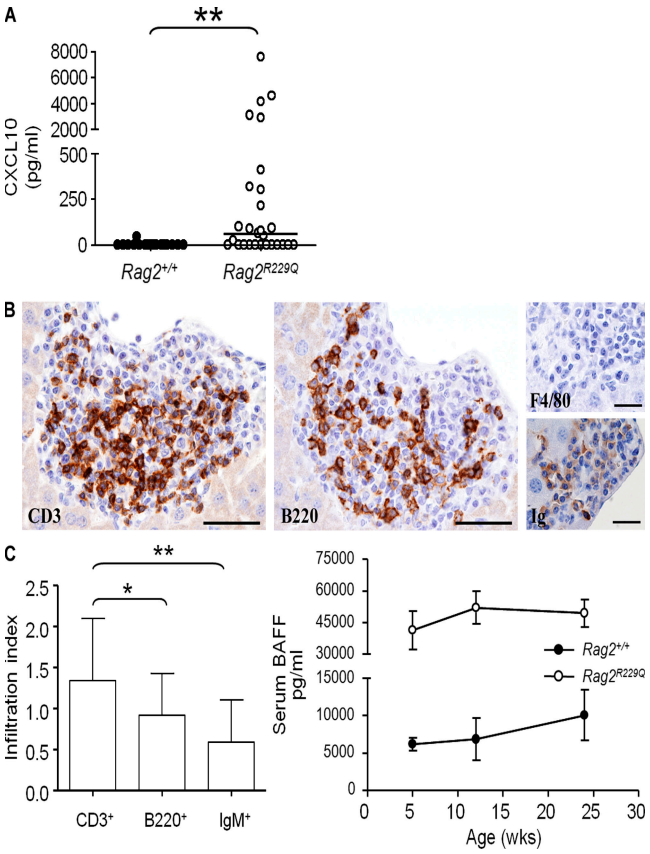

Figure S6. Characterization of autoimmune-like manifestations in *Rag2*^{R229Q} mice. (A) *Rag2*^{R229Q} mice have elevated serum levels of CXCL10. Serum CXCL10 levels in WT (n = 17) and *Rag2*^{R229Q} (n = 28) littermates (10–16 wk old), measured by ELISA. For each serum sample, three replicates were run and three independent experiments were performed. (B) Characterization of liver infiltrates show positive staining for CD3, B220, and Ig. The monocytes/macrophages marker F4/80 resulted negative. Scale bars correspond to 50 μM. (C) Analysis of CD3, B220, IgM positive cell infiltrates in different organs (gut, liver, lung, kidney and skin) of mutant mice (n = 20). The degree of cell infiltration was scored as described in Materials and methods and shown as Infiltration Index. (D) Serum BAFF in different aged WT and *Rag2*^{R229Q} mice, as measured by ELISA. For each time point the mean values ± SD of concentrations from n = 5 (WT) or n = 8–9 (*Rag2*^{R229Q}) mice are shown. The results are representative of three independent experiments.

SUPPLEMENTAL MATERIAL

Cassani et al., http://www.jem.org/cgi/content/full/jem.200091928/DC1

Table S1. Clinical and genetic features of patients with Omenn syndrome

	OS1	OS2	OS3	OS4	OS5	OS6	HD range values
Age at onset	1 wk	2 mo	1 wk	2 mo	3.5 mo	13 mo	
Skin lesions	+	+	+	+	+	+	
Hepatosplenomegaly	+	+	+	+	n.a.	-	
Colitis	-	-	-	-	-	-	
Lymphadenopathy	+	+	+	+	n.a.	-	
Eosinophilia	+	+	+	+	+	-	
CD3 (cells/µl)	10491	8607	1840	2700	100	40	2,014–6,954
CD19 (cells/µl)	2	2	4	60	10	10	411–2,972
IgM (mg/dl)	8	7	n.a.	45	32	6	41–228
IgG (mg/dl)	#	#	380	822	293	173	172–1,430
IgE (UI/ml)	-	>5000	2200	139	n.a.	n.a.	(n.v. <20 UI/ml
RAG1 mutation	Allele 1: c.424C>T Allele 2: c.1373delT	Allele 1: c.256_257delAA Allele 2: c.1373delT	Allele 1 and 2: c.519delT	Allele 1 and 2: c.256_257delAA	Allele 1: c.2487G>T;c.2488A>T Allele 2: c.2701_2705delCCTGC	Allele 1: c.256_257delAA Allele 2: c.1331C>T	
Effect on RAG1 protein	p.Arg142X p.Met458SerfsX34	p.Lys86ValfsX33 p.Glu722Lys	p.Glu174SerfsX14	p.Lys86ValfsX33	p.Arg829Ser;p.Lys830X p.Pro901X	p.Lys86ValfsX33 p.Ala444Val	

n.a., not analyzed. Mutation nomenclature according to the guidelines of the human genome variation society (www.hgvs.org) using M29474 as reference sequence for *RAG1*. Position 1 corresponds to the A of the ATG initiation codon.

[#]Patient receiving IVIG at the time of the analysis.

Table S2. Repertoire of IgM+ splenic B cells

Mouse sample no.	Sorted population	Igh-V	Igh-V family	Igh-D	Igh-J	Igh CDR3	Igh hyper	Cluster	Igh CDR3 length
bulk R229Q #1	B220+	VH36-60.a2.90	36-60	DSP2.9	JH1	ARWLLQYWYFDV	0	7	12
bulk R229Q #1	B220+	VH36-60.a2.90	36-60	DSP2.9	JH1	ARWLLRYWYFDV	0	7	12
bulk R229Q #1	B220+	VH36-60.a2.90	36-60	DSP2.9	JH1	ARWLLQYWYFDV	0	7	12
bulk R229Q #1	B220+	VH36-60.a2.90	36-60	DSP2.9	JH1	ARWLLRYWYFDV	0	7	12
bulk R229Q #1	B220+	VH36-60.a2.90	36-60	DSP2.9	JH1	ARWLLQYWYFDV	0	7	12
bulk R229Q #1	B220+	VHQ52.a27.79	Q52	DQ52-BALB/c	JH2	AREAPNWDGYFDY	0	0	13
bulk R229Q #1	B220+	VH36-60.a2.90	36-60	DSP2.9	JH1	ARWLLQYWYFDV	0	7	12
bulk R229Q #1	B220+	VHSM7.a3.93	SM7	DSP2.5	JH4	ARPNGNYVYYSMDY	3	0	14
bulk R229Q #1	B220+	VH7183.a19.31	7183	-	JH2	ARRQLAY	0	0	7
bulk R229Q #1	B220+	J558.20	J558	-	JH2	ARRVEGFDY	0	2	9
bulk R229Q #1	B220+	VH36-60.a2.90	36-60	DSP2.9	JH1	ARWLLQYWYFDV	0	7	12
bulk R229Q #1	B220+	VH7183.a21.35	7183	DQ52-C57BL/6	JH3	ARGLTGTAVFAY	0	10	12
bulk R229Q #1	B220+	VH36-60.a2.90	36-60	DSP2.9	JH1	ARWLLQYWYFDV	0	7	12
bulk R229Q #1	B220+	VH7183.a4.6	7183	-	JH2	AREDY	0	11	5
bulk R229Q #1	B220+	VHQ52.a3.8	Q52	-	JH1	AKVDV	0	0	5
bulk R229Q #1	B220+	VH7183.a21.35	7183	DQ52-C57BL/6	JH3	ARGLTGTAVFAY	0	10	12
bulk R229Q #1	B220+	VH36-60.a2.90	36-60	DSP2.9	JH1	ARWLLQYWYFDV	0	7	12
bulk R229Q #1	B220+	VH7183.a47.76	7183	-	JH2	ARDGTESYFDY	1	0	11
bulk R229Q #1	B220+	VH36-60.a2.90	36-60	DSP2.9	JH1	ARWLLQYWYFDV	0	7	12
bulk R229Q #1	B220+	VH36-60.a2.90	36-60	DSP2.9	JH1	ARWLLQYWYFDV	0	7	12
bulk R229Q #1	B220+	J558.70pg.171	J558	DQ52-C57BL/6	JH3	ALGRFAY	11	0	7
bulk R229Q #1	B220+	VH36-60.a2.90	36-60	DSP2.9	JH1	ARWLLQYWYFDV	0	7	12
bulk R229Q #1	B220+	VH36-60.a2.90	36-60	DSP2.9	JH1	ARWLLQYWYFDV	0	7	12
bulk R229Q #1	B220+	VH36-60.a8.117	36-60	DQ52-C57BL/6	JH1	ARYKWDVYFDV	1	0	11
bulk R229Q #1	B220+	VH36-60.a2.90	36-60	DSP2.9	JH1	ARWLLQYWYFDV	0	7	12
bulk R229Q #1	B220+	VH7183.a21.35	7183	DFL16.1	JH3	ARALIRGAWFAY	0	0	12
bulk R229Q #1	B220+	VH36-60.a2.90	36-60	DSP2.9	JH1	ARWLLQYWYFDV	0	7	12
bulk R229Q #1	B220+	VH7183.a46.75	7183	-	JH2	AREGGRQGAFDY	2	0	12
bulk R229Q #1	B220+	VH36-60.a8.117	36-60	DFL16.1	JH1	ARYYGSSYWYFDV	0	0	13
bulk R229Q #1	B220+	VH36-60.a2.90	36-60	-	JH2	AKSQSYYFDY	1	8	10

bulk R229Q #1	B220+	J558.20	J558	-	JH2	ARRVEGFDY	1	2	9
bulk R229Q #1	B220+	VH36-60.a2.90	36-60	DSP2.9	JH1	ARWLLQYWYFDV	0	7	12
bulk R229Q #1	B220+	VH36-60.a2.90	36-60	DSP2.5	JH2	ARNYGKRGRYYFDY	2	0	14
bulk R229Q #1	B220+	VH36-60.a2.90	36-60	DSP2.9	JH1	ARWLLQYWYFDV	2	7	12
bulk R229Q #1	B220+	VH36-60.a2.90	36-60	DSP2.9	JH1	ARWLLQYWYFDV	0	7	12
bulk R229Q #1	B220+	VH36-60.a2.90	36-60	DSP2.9	JH1	ARWLLQYWYFDV	0	7	12
bulk R229Q #1	B220+	VH36-60.a2.90	36-60	-	JH2	AKSQSYYFDY	2	8	10
bulk R229Q #1	B220+	VH36-60.a2.90	36-60	DSP2.9	JH1	ARWLLQYWYFDV	0	7	12
bulk R229Q #1	B220+	VH7183.a4.6	7183	-	JH2	AREDY	0	11	5
bulk R229Q #1	B220+	VH36-60.a2.90	36-60	DSP2.9	JH1	ARWLLQYWYFDV	0	7	12
bulk R229Q #1	B220+	VH36-60.a2.90	36-60	DSP2.9	JH1	ARWLLQYWYFDV	0	7	12
bulk R229Q #1	B220+	J558.70pg.171	J558	DQ52-BALB/c	JH2	ARLGQGGYYFDY	11	0	12
bulk R229Q #1	B220+	J558.47	J558	DQ52-BALB/c	JH3	AREGWDGFAY	0	0	10
bulk R229Q #2	B220+	Vh10.2a	VH10	-	JH1	VRRAQLYWYFDV	0	6	12
bulk R229Q #2	B220+	Vh10.2a	VH10	-	JH1	VRRAQLYWYFDV	0	6	12
bulk R229Q #2	B220+	Vh10.2a	VH10	-	JH1	VRRAQLYWYFDV	1	6	12
bulk R229Q #2	B220+	Vh10.2a	VH10	-	JH1	VRRAQLYWYFDV	1	6	12
bulk R229Q #2	B220+	SM7.4.63	SM7	DSP2.5	JH3	TVYYGNYWFAY	0	0	11
bulk R229Q #2	B220+	VH36-60.a2.90	36-60	DQ52-C57BL/6	JH3	ARSRWDGGFAY	2	9	11
bulk R229Q #2	B220+	Vh10.2a	VH10	-	JH1	VRRAQLYWYFDV	1	6	12
bulk R229Q #2	B220+	VH36-60.a2.90	36-60	DQ52-C57BL/6	JH3	ARSRWDGGFAY	3	9	11
bulk R229Q #2	B220+	VH7183.a19.31	7183	DQ52-C57BL/6	JH3	ARGAGTAFAY	0	0	10
bulk R229Q #2	B220+	Vh10.2a	VH10	-	JH1	VRRAQLYWYFDV	0	6	12
bulk R229Q #2	B220+	J558.17	J558	DFL16.2	JH2	ARRLFDY	0	0	7
bulk R229Q #2	B220+	Vh10.2a	VH10	-	JH1	VRRAQLYWYFDV	0	6	12
bulk R229Q #2	B220+	VH7183.a7.10	7183	-	JH2	ARQNWDY	1	0	7
bulk R229Q #2	B220+	Vh10.2a	VH10	-	JH1	VRRAQLYWYFDV	0	6	12
bulk R229Q #2	B220+	Vh10.2a	VH10	-	JH1	VRRAQLYWYFDV	0	6	12
bulk R229Q #2	B220+	Vh10.2a	VH10	-	JH1	VRRAQLYWYFDV	0	6	12
bulk R229Q #2	B220+	Vh10.2a	VH10	-	JH1	VRRAQLYWYFDV	0	6	12
bulk R229Q #2	B220+	Vh10.2a	VH10	-	JH1	VRRAQLYWYFDV	0	6	12
bulk R229Q #2	B220+	J558.45	J558	-	JH2	ARWGY	1	3	5
bulk R229Q #2	B220+	Vh10.2a	VH10	-	JH1	VRRAQLYWYFDV	1	6	12
bulk R229Q #2	B220+	Vh10.2a	VH10	-	JH1	VRRAQLYWYFDV	1	6	12
bulk R229Q #2	B220+	Vh10.2a	VH10	-	JH1	VRRAQLYWYFDV	0	6	12

bulk R229Q #2	B220+	VHQ52.a17.46	Q52	-	JH3	AKNEGDVWFAY	7	0	11
bulk R229Q #2	B220+	VH36-60.a1.85	36-60	-	JH2	ARSSQYYFDY	1	0	10
bulk R229Q #2	B220+	Vh10.2a	VH10	-	JH1	VRRAQLYWYFDV	0	6	12
bulk R229Q #2	B220+	Vh10.2a	VH10	-	JH1	VRRAQLYWYFDV	0	6	12
bulk R229Q #2	B220+	J558.44	J558	-	JH2	ARKLRYFDY	0	12	9
bulk R229Q #2	B220+	Vh10.2a	VH10	-	JH1	VRRAQLYWYFDV	1	6	12
bulk R229Q #2	B220+	J558.45	J558	-	JH2	ARWGY	2	3	5
bulk R229Q #2	B220+	Vh10.2a	VH10	-	JH1	VRRAQLYWYFDV	0	6	12
bulk R229Q #2	B220+	VH7183.a30.50	7183	DQ52-C57BL/6	JH2	ARSPLTGTNYFDY	0	0	13
bulk R229Q #2	B220+	J558.44	J558	-	JH2	ARKLRYFDY	0	12	9
bulk R229Q #2	B220+	Vh10.2a	VH10	-	JH1	VRRAQLYWYFDV	0	6	12
bulk R229Q #2	B220+	J558.52	J558	DSP2.5	JH2	ARGYGNYVFDY	0	0	11
bulk R229Q #2	B220+	J558.44	J558	-	JH2	ARKLRYFDY	0	12	9
bulk R229Q #2	B220+	Vh10.2a	VH10	-	JH1	VRRAQLYWYFDV	1	6	12
bulk WT	B220+	J558.2.88	J558	DFL16.1	JH4	ARGNYYGSKAMDY	0	0	13
bulk WT	B220+	Vh10.2b	VH10	DFL16.1	JH1	VRQGYYYGSSYDWYFDV	0	0	17
bulk WT	B220+	VH7183.a7.10	7183	DFL16.1	JH1	ARPPYYGSSYYFDV	0	0	14
bulk WT	B220+	J558.83.189	J558	DST4-C57BL/6	JH3	ARRAQATWFAY	0	4	11
bulk WT	B220+	J558.39.129	J558	-	JH2	ARWGSQGYFDY	0	0	11
bulk WT	B220+	SM7.4.63	SM7	DFL16.1	JH1	TTDYGSSYWYFDV	0	0	13
bulk WT	B220+	7183.4.6	7183	DFL16.1	JH1	ARSYGSSYWYFDV	0	0	13
bulk WT	B220+	J558.84.190	J558	DFL16.1	JH4	ARSSSYAMDY	0	0	10
bulk WT	B220+	7183.20.37	7183	DSP2.13	JH4	ARGGDYVDYAMDY	1	0	13
bulk WT	B220+	7183.20.37	7183	DSP2.9	JH4	ARGGYYPYYAMDY	1	0	13
bulk WT	B220+	J558.83.189	J558	DST4-C57BL/6	JH3	AGRAQATWFAY	0	4	11
bulk WT	B220+	Q52.13.40	Q52	DST4-C57BL/6	JH1	AKRGSRRQLWYFDV	1	0	14
bulk WT	B220+	Vh10.2b	VH10	DSP2.9	JH2	VRGDGYSFDY	1	0	10
bulk WT	B220+	J558.85.191	J558	-	JH4	AKGGKYYAMDY	2	0	11
bulk WT	B220+	7183.20.37	7183	DSP2.2	JH4	ARNDYDEGYAMDY	3	0	13
bulk WT	B220+	J558.85.191	J558	DSP2.2	JH3	AKPIYYDYAWFAY	0	0	13
bulk WT	B220+	SM7.4.63	SM7	DFL16.1	JH3	TIIDYYGSSRFAY	0	0	13
bulk WT	B220+	Q52.3.8	Q52	-	JH3	AKAGGFAY	0	0	8
bulk WT	B220+	SM7.2.49	SM7	DFL16.1	JH2	ARGITTVVGDY	0	0	11
bulk WT	B220+	Vh10.2b	VH10	DSP2.2	JH4	VRLDYDRAMDY	2	0	11
bulk WT	B220+	VH7183.a7.10	7183	DFL16.1j	JH4	ARQGLFTEDYAMDY	0	0	14

bulk WT	B220+	J558.85.191	J558	-	JH2	ASSGSLYYFDY	0	0	11
bulk WT	B220+	J558.84.190	J558	DFL16.1	JH3	ARLMDYGSSFAY	1	0	12
bulk WT	B220+	J558.6.96	J558	DST4-C57BL/6	JH4	ARRKDSSGYDYYAMDY	1	0	16
bulk WT	B220+	VH7183.a7.10	7183	DSP2.9	JH2	ARHGGWLPSFDY	0	0	12
bulk WT	B220+	J558.4.93	J558	DQ52-C57BL/6	JH2	AREENWDGDY	0	0	10
bulk WT	B220+	J558.85.191	J558	DST4-C57BL/6	JH2	ARQLRLLDY	0	0	9
bulk WT	B220+	J558.6.96	J558	DSP2.x	JH1	ASGSNYVWYFDV	0	0	12
bulk WT	B220+	J558.39.129	J558	-	JH4	ARRGLTEAMDY	0	0	11
bulk WT	B220+	J558.39.129	J558	DQ52-C57BL/6	JH4	ARKLGLYYAMDY	0	0	12
bulk WT	B220+	J558.69.170	J558	DFL16.1	JH2	ARNRIAVVAKGY	0	0	12
bulk WT	B220+	VH7183.a7.10	7183	DSP2.9	JH3	ARHGGGYYVFAY	0	0	12
bulk WT	B220+	Q52.3.8	Q52	DSP2.x	JH4	AKPWAYYSNYYAMDY	0	0	15
bulk WT	B220+	J558.85.191	J558	DFL16.1	JH2	ARFYYYGSKGYFDY	1	0	14
bulk WT	B220+	7183.20.37	7183	DFL16.1	JH2	ARYYYGSSYFDY	0	0	12
bulk WT	B220+	J558.6.96	J558	-	JH2	ARVESYTADY	9	0	10
bulk WT	B220+	7183.4.6	7183	DFL16.1	JH1	ARVYGSSWYFDV	1	0	12
bulk WT	B220+	36-60.6.70	36-60	DSP2.x	JH3	ATYSNYAWFAY	0	0	11
bulk WT	B220+	Q52.8.22	Q52	DFL16.1	JH4	ARHRSSYAYAMDY	1	0	13
bulk WT	B220+	7183.20.37	7183	-	JH1	ARHDSWYFDV	1	0	10
bulk WT	B220+	J558.84.190	J558	DQ52-C57BL/6	JH2	ARSNWDYFDY	0	0	10
bulk WT	B220+	Q52.3.8	Q52	DFL16.1	JH1	AKQGLFTTVVADWYFDV	0	5	17
bulk WT	B220+	J558.22.112	J558	DFL16.1	JH2	ARSRGSYYYFDY	0	0	12
bulk WT	B220+	VH10.3.91	VH10	DFL16.1	JH2	VREGTTVGSDY	1	0	11
bulk WT	B220+	7183.20.37	7183	DSP2.9	JH2	ARHGGWLPSFDY	5	1	12
bulk WT	B220+	VH7183.a7.10	7183	DSP2.x	JH1	ARQNSKGYFDV	1	0	11
bulk WT	B220+	VH7183.a7.10	7183	DFL16.1	JH2	ARYYYGSSYFDY	1	0	12
bulk WT	B220+	VH7183.a7.10	7183	DFL16.1	JH1	ARHPYYYGSSCWYFDV	0	0	16
bulk WT	B220+	7183.20.37	7183	DSP2.9	JH2	ARHGGWLPSFDY	5	1	12
bulk WT	B220+	Q52.7.18	Q52	-	JH2	AKEDFDY	0	13	7
bulk WT	B220+	VH10.3.91	VH10	-	JH2	VRGWGFDY	0	0	8
bulk WT	B220+	J558.4.93	J558	DSP2.9	JH1	ARGDGYYHWYFDV	0	0	13
bulk WT	B220+	Q52.3.8	Q52	DFL16.1	JH1	AKQGLFTTVVADWYFDV	0	5	17
bulk WT	B220+	Q52.7.18	Q52	-	JH2	AKEDFDY	0	13	7
cell sort R229Q #1	B220+ CD19+	VHQ52.a19.61	Q52	-	JH2	ARGGPSSALDY	0	0	11
cell sort R229Q #1	B220+ CD19+	J558.16.106	J558	DSP2.x	JH2	ARGSNYFDY	0	0	9

cell sort R229Q #1	B220+ CD19+	J558.1.85	J558	DSP2.2	JH3	AYYDYDEWFAY	1	14	11
cell sort R229Q #1	B220+ CD19+	VH36-60.a2.90	36-60	DFL16.1	JH2	ARRVVFDY	0	0	8
cell sort R229Q #1	B220+ CD19+	VH36-60.a6.114	36-60	-	JH3	ARGNAWFAY	0	0	9
cell sort R229Q #1	B220+ CD19+	J558.1.85	J558	DSP2.2	JH3	AYYDYDEWFAY	1	14	11
cell sort R229Q #1	B220+ CD19+	J558.20	J558	-	JH3	ASGVPPWFAY	0	0	10
cell sort R229Q #1	B220+ CD19+	J558.55.149	J558	DFL16.1	JH1	ARIYYGSSYWYFDV	0	15	14
cell sort R229Q #1	B220+ CD19+	J558.55.149	J558	DFL16.1	JH1	ARIYYGSSYWYFDV	0	15	14
cell sort R229Q #1	B220+ CD19+	J558.50	J558	DQ52-BALB/c	JH2	TIQTGTFDY	0	0	9
cell sort R229Q #1	B220+ CD19+	VHSM7.a1.83	SM7	DSP2.10	JH2	ARVGYRYDFDY	0	0	11
cell sort R229Q #1	B220+ CD19+	VHS107.a3.106	S107	-	JH2	ARDTFFDY	0	0	8
cell sort R229Q #1	B220+ CD19+	J558.12.102	J558	DSP2.9	JH2	TRDDGYFDY	8	0	9
cell sort R229Q #2	B220+ CD19+	J558.45	J558	-	JH3	ARSTSQLFAY	1	0	10
cell sort R229Q #2	B220+ CD19+	J558.17	J558	DQ52-BALB/c	JH2	ARDGTGGFDY	0	0	10
cell sort R229Q #2	B220+ CD19+	VH7183.a7.10	7183	DFL16.1	JH4	ARHEDNYVTRAMDY	4	17	14
cell sort R229Q #2	B220+ CD19+	VH7183.a19.31	7183	DQ52-C57BL/6	JH2	ASSNWDGFDY	0	0	10
cell sort R229Q #2	B220+ CD19+	J558.29	J558	DSP2.2	JH3	AREEGLRPWFAY	0	0	12
cell sort R229Q #2	B220+ CD19+	VH7183.a7.10	7183	DSP2.9	JH4	ARHEGNYVTRAMDY	0	17	14
cell sort R229Q #2	B220+ CD19+	VHJ606.a6.127#	J606	DSP2.13	JH2	TRTGDYFDY	0	0	9
cell sort R229Q #2	B220+ CD19+	VH36-60.a8.117	36-60	DSP2.10	JH3	ASYYRYDAGFAY	1	0	12
cell sort R229Q #2	B220+ CD19+	VH7183.a7.10	7183	DSP2.9	JH4	ARHEGNYVTRAMDY	1	17	14
cell sort R229Q #2	B220+ CD19+	J558.77.180	J558	-	JH2	ARRSLYYFDY	14	0	10
cell sort R229Q #2	B220+ CD19+	J558.47	J558	-	JH2	ARGVLHFDN	2	16	9
cell sort R229Q #2	B220+ CD19+	VH7183.a7.10	7183	DSP2.9	JH4	ARHEGNYVTGAMDY	0	17	14
cell sort R229Q #2	B220+ CD19+	VH36-60.a1.85	36-60	DSP2.13	JH2	ARLGRYYFDY	0	0	10
cell sort R229Q #2	B220+ CD19+	J558.50	J558	-	JH2	TRSFLGTDY	0	0	9
cell sort R229Q #2	B220+ CD19+	J558.47	J558	-	JH2	ARGVLHFDY	6	16	9
cell sort R229Q #3	B220+ CD19+	VHS107.a3.106	S107	DSP2.10	JH1	ARDDRYGVDWYFDV	0	0	14
cell sort R229Q #3	B220+ CD19+	J558.47	J558	-	JH2	ARLGY	0	0	5
cell sort R229Q #3	B220+ CD19+	VH7183.a47.76	7183	-	JH2	ARGLYYFDY	0	0	9
cell sort R229Q #3	B220+ CD19+	VHQ52.a27.79	Q52	DSP2.5	JH2	AREGGGNYDYFDY	0	0	13
cell sort R229Q #3	B220+ CD19+	J558.79.184	J558	-	JH4	ARGAMDY	17	0	7
cell sort R229Q #3	B220+ CD19+	VHA1	J558	DQ52-C57BL/6	JH1	ARSRLTGYWYFDV	0	0	13
cell sort WT #1	B220+ CD19+	J558.8	J558	DSP2.3	JH3	ASSLYYPFAY	1	0	10
cell sort WT #1	B220+ CD19+	J558.51	J558	DSP2.9	JH4	RIGYYGDYYAMDY	6	0	13
cell sort WT #1	B220+ CD19+	VHSM7.a3.93	SM7	DSP2.2	JH3	ARWYDYPFAY	0	0	10

cell sort WT #1	B220+ CD19+	J558.k	J558	DFL16.1	JH3	KRSGITTVY	0	0	9
cell sort WT #1	B220+ CD19+	J558.79.184	J558	DSP2.3	JH3	ARENYGYSFA	0	0	10
cell sort WT #1	B220+ CD19+	Q52.8.22	Q52	DFL16.1	JH4	ARDYYGSSYDAMDY	0	0	14
cell sort WT #1	B220+ CD19+	J558.i	J558	DFL16.1	JH4	ARSGTTVVAPYAMDY	0	0	15
cell sort WT #1	B220+ CD19+	VH36-60.a6.114	36-60	-	JH2	AREVYFDY	0	0	8
cell sort WT #1	B220+ CD19+	J558.26.116	J558	DFL16.2	JH3	ARPVTTATFAY	4	0	11
cell sort WT #1	B220+ CD19+	J558.23	J558	-	JH2	ASRDY	1	0	5
cell sort WT #1	B220+ CD19+	J606.4.82	J606	DSP2.5	JH3	TRPLYYFAY	0	0	9
cell sort WT #1	B220+ CD19+	J558.51	J558	DSP2.10	JH1	TPYRYDYWYFDV	0	0	12
cell sort WT #1	B220+ CD19+	J558.33	J558	DFL16.1	JH1	ARSGDPYYGGGFDV	0	0	14
cell sort WT #2	B220+ CD19+	J558.50	J558	-	JH3	TRSEDYAPFAY	4	0	11
cell sort WT #2	B220+ CD19+	VHS107.a3.106	S107	-	JH2	ARDGYFDY	0	0	8
cell sort WT #2	B220+ CD19+	J558.8	J558	DSP2.5	JH4	ARFLWDYYAMDY	1	0	12
cell sort WT #2	B220+ CD19+	VHS107.a3.106	S107	-	JH4	ARVKDFYYYAMDY	0	0	13
cell sort WT #2	B220+ CD19+	VH36-60.a6.114	36-60	DFL16.1	JH4	ARGGGLLGAMDY	0	0	12
cell sort WT #2	B220+ CD19+	VHQ52.a27.79	Q52	DSP2.9	JH3	ARGGGYYLFAY	0	0	11
cell sort WT #2	B220+ CD19+	VHQ52.a2.4	Q52	-	JH3	ARNGLFAY	0	0	8
cell sort WT #2	B220+ CD19+	VHQ52.a27.79	Q52	DFL16.1j	JH4	ARDYLYGRAMDY	0	0	12
cell sort WT #2	B220+ CD19+	VH7183.a7.10	7183	DSP2.2	JH4	ARHRDYLYAMDY	0	0	12
cell sort WT #2	B220+ CD19+	J558.17	J558	DFL16.1j	JH3	ARLSSTAGATY	0	0	11
cell sort WT #2	B220+ CD19+	J558.40	J558	DFL16.2	JH4	TRQITTPFYAMDY	1	0	13
cell sort WT #2	B220+ CD19+	VHQ52.a27.79	Q52	DFL16.1	JH4	ARGPLITTVVATGYYAMDY	0	0	19
cell sort WT #3	B220+ CD19+	VHSM7.a4.108	SM7	DFL16.1	JH2	NAGPVLYYYGSSFYYFDY	0	0	18
cell sort WT #3	B220+ CD19+	J558.19.109	J558	DFL16.1	JH4	ARSPITTVGDY	2	0	11
cell sort WT #3	B220+ CD19+	VHQ52.a24.72	Q52	DSP2.2	JH4	ARDDYDYAMDY	0	0	11
cell sort WT #3	B220+ CD19+	J558.3.90	J558	DFL16.2	JH2	TKTTNILYYFDY	0	0	12
cell sort WT #3	B220+ CD19+	J558.47	J558	DSP2.3	JH3	ARDYGYDGCFAY	0	0	12
cell sort WT #3	B220+ CD19+	SM7.4.63	SM7	DST4-C57BL/6	JH4	TRPTAQAPGYYAMDY	1	0	15
cell sort WT #3	B220+ CD19+	J558.64.162	J558	DSP2.9	JH4	ARHDPLYDGPSMDY	1	0	14
cell sort WT #3	B220+ CD19+	Q52.3.8	Q52	DSP2.3	JH3	AKLDGYDEGFAY	0	0	12